Dominance modifiers at the Arabidopsis self-incompatibility locus retain proto-miRNA features and act through non-canonical pathways

Rita A Batista, Eléonore Durand, Monika Mörchen, Jacinthe Azevedo-Favory, Samson Simon, Manu Dubin, Vinod Kumar, Eléanore Lacoste, Corinne Cruaud, Christelle Blassiau, et al.

Dominance modifiers at the Arabidopsis self-incompatibility locus retain proto-miRNA features and act through non-canonical pathways

Rita A. Batista[1,a], Eléonore Durand[1], Monika Mörchen[1], Jacinthe Azevedo-Favory[2], Samson Simon[1], Manu Dubin[1], Vinod Kumar[3], Eléanore Lacoste[4], Corinne Cruaud[5], Christelle Blassiau[1], Matteo Barois[1], Anne-Catherine Holl[1], Chloé Ponitzki[1], Nathalie Faure[1], William Marande[6], Sonia Vautrin[6], Isabelle Fobis-Loisy[7], Jean-Marc Aury[4], Sylvain Legrand[1], Ute Krämer[3], Thierry Lagrange[2], Xavier Vekemans[1], Vincent Castric[1]

1. Univ. Lille, CNRS, UMR 8198 – Evo-Eco-Paleo, F-59000 Lille, France
2. CNRS, Laboratoire Génome et Développement des Plantes, UMR 5096, 66860 Perpignan, France, and Université Perpignan *Via Domitia*, Laboratoire Génome et Développement des Plantes, UMR 5096, F-66860 Perpignan, France
3. Department of Molecular Genetics and Physiology of Plants, Faculty of Biology and Biotechnology, Ruhr University Bochum, D-44801 Bochum, Germany
4. Génomique Métabolique, Genoscope, Institut François Jacob, CEA, CNRS, Univ Evry, Université Paris-Saclay, 91057 Evry, France
5. Genoscope, Institut François Jacob, CEA, Université Paris-Saclay, Evry, 91057, France
6. INRAE - CNRGV French Plant Genomic Resource Center - Castanet Tolosan, France
7. Laboratoire Reproduction et Développement des Plantes, Université de Lyon, ENS de Lyon, UCB Lyon 1, CNRS, INRAE, F-69342 Lyon, France

a. Current address: Max Planck Institute for Biology, Department of Algal Development and Evolution, 72076 Tübingen, Germany

Corresponding author: Vincent Castric, vincent.castric@univ-lille.fr

Author Contributions: Designed research – RAB, ED, MM, JA-F, MD, SS, VK, IF-L, J-MA, SL, UK, TL, XV, VC; Performed research – RAB, ED, MM, JA-F, MD, SS, VK, EL, CC, CB, A-CH, CP, NF, IF-L; Contributed new reagents or analytic tools – WM, SV, IF-L, J-MA, UK, TL, XV, VC; Analyzed data – RAB, ED, MM, JA-F, MD, SS, VK, EL, J-MA, SL, XV, VC; Wrote the paper – RAB, VC. All authors reviewed and edited the manuscript.

Classification: Biological Sciences, Plant Biology

Keywords: self-incompatibility; dominance; miRNA; gene silencing

This PDF file includes:

Main Text

Figures 1 to 5, with corresponding supplementary figures

Abstract

Self-incompatibility in flowering plants is a common mechanism that prevents self-fertilization and promotes outcrossing. In Brassicaceae, there is high genetic diversity at the locus controlling self-incompatibility, and dozens of distinct alleles are organized in a complex dominance hierarchy: the gene controlling self-incompatibility specificity in pollen shows monoallelic expression in heterozygote individuals. This is achieved through the action of sRNA precursors that resemble miRNAs, although the underlying molecular mechanisms remain elusive. Here, we engineered *Arabidopsis thaliana* lines expressing components of the *Arabidopsis halleri* self-incompatibility system, and used a reverse genetics approach to pinpoint the pathways underlying the function of these sRNA precursors. We showed that they trigger a robust decrease in transcript abundance of the recessive pollen self-incompatibility genes, but not through the canonical transcriptional or post-transcriptional gene silencing pathways. Furthermore, we observed that single sRNA precursors are typically processed into hundreds of sRNA molecules of distinct sizes, abundance levels and ARGONAUTE loading preferences. This heterogeneity closely resembles that of proto-miRNAs, the evolutionary ancestors of miRNAs. Our results suggest that these apparently arbitrary features, which are often associated with lack of effects on gene expression, are crucial in the context of the self-incompatibility dominance hierarchy since they allow for one sRNA precursor of a given allele to repress multiple other recessive alleles. This study not only provides an in-depth characterization of the molecular features underlying complex dominance interactions, but also constitutes a unique example of how specific evolutionary constraints shape the progression of sRNA precursors along the proto-miRNA - miRNA evolutionary continuum.

Significance statement

miRNAs are genetically encoded small non-coding RNA molecules that control gene expression. Here, we characterized a set of regulatory loci present in the self-incompatibility locus of *Arabidopsis halleri* which resemble proto-miRNAs, the evolutionary ancestors of miRNAs. We report that despite the absence of classical miRNA features thought to be essential for gene expression regulation, proto-miRNAs generated by these loci robustly repress the activity of self-incompatibility genes through non-canonical silencing pathways, and thus function to establish a complex dominance hierarchy between self-incompatibility alleles. We show that the evolutionary forces promoting diversity of self-incompatibility alleles have likely favored the maintenance of proto-miRNA features in order to mediate dominance interactions between numerous alleles, thus preventing the transition of self-incompatibility proto-miRNAs into canonical miRNAs.

Main text

Introduction

Genetic dominance is the widespread property by which one allele can mask the phenotypic effect of another in a heterozygous genotype **(1)**. Dominance introduces non-linearity in the genotype-to-phenotype map and influences the exposure of mutations to natural selection, thus altering the probability and dynamics of their fixation, elimination, or maintenance in natural populations **(2)**. The evolution of dominance has been subject to a fierce debate in the field of genetics throughout the 20th century **(3)**, specifically around the existence of genetic elements dedicated to altering the dominance of other alleles in *trans* **(4)**, and the possibility for natural selection to act effectively on these elements **(5)**. The existence of these dominance modifiers has remained elusive for many years; nevertheless, theoretical studies have predicted that dominance modifiers could exist in cases where heterozygosity is high, such as in Batesian and Müllerian mimicry in butterflies, or at the self-incompatibility locus of Brassicaceae plants **(3)**. More recently, dominance modifiers similar to those envisioned by Fisher **(4)** were empirically identified at the self-incompatibility locus of Brassica and Arabidopsis **(6–8)**. However, their mode of action and evolutionary properties remain elusive.

Self-incompatibility is a widespread self-recognition mechanism in hermaphroditic flowering plants that prevents selfing and enforces outcrossing. In Brassicaceae, self-pollen recognition is controlled at the sporophytic level by a single non-recombining self-incompatibility locus (*S*-locus) containing two protein-coding genes: one encoding a trans-membrane receptor (SRK) expressed in papillae cells as the female component, and the male component consisting of an SCR peptide produced in the tapetum of the anther and deposited on the surfaces of the pollen grains. The SRK and SCR proteins function as a receptor-ligand system, such that pollen germination is stopped when a pair of cognate SRK and SCR proteins interact upon pollen deposition on the pistil, ultimately preventing fertilization **(9–13)**. The *S*-locus is subject to an intense long-term balancing selection, which favors the maintenance of a high number of distinct *S*-alleles **(14–17)**. Although heterozygosity is typically very high at the *S*-locus, monoallelic expression of the male *SCR* gene is the rule, following a transitive and mostly linear dominance hierarchy among *S*-alleles **(18–20)**. These dominance interactions maximize reproductive fitness, since repressing one of the two *S*-alleles carried by a diploid heterozygous male individual avoids rejection by pistils expressing the same allelic specificity, and thus maximizes the number of available female partners **(21)**. In *Arabidopsis lyrata* and *A. halleri*, respectively, 56 and 43 *S*-alleles have been documented so far **(15, 22)**, and are divided in four main dominance classes, with class IV being the most dominant and class I the most recessive **(23, 24)**.

Underlying these dominance interactions are *S*-locus dominance modifiers, which take the form of sRNA generating loci. Similarly to miRNAs genes, these loci are transcribed into an RNA molecule that folds into a hairpin structure, which is subsequently cleaved into sRNAs. In *A. halleri,* eight distinct families of sRNA precursors exist, and they are predicted to control dominance interactions between and within the four *S*-allele dominance classes **(6)**. Interestingly, in Brassica where only two dominance classes exist, only two sRNA precursors genes have been identified **(7, 8, 20)**, suggesting that there is an association between the complexity of the dominance network and the total number

of dominance modifiers. The two sRNA precursors of Brassica (*Smi* and *Smi2*) have each been suggested to form a hairpin and produce a 24-nt sRNA with sequence similarity to the 5' region of *SCR* (referred to *SP11* in the Brassica nomenclature). The presence of this sRNA is associated with decreased expression of the recessive *SCR* allele as well as deposition of DNA methylation at the targeted region in the tapetum cells **(7, 8, 20)**. This is reminiscent of what is observed in several plant species where 21/24-nt sRNAs derived from miRNAs genes or inverted repeats can be loaded onto proteins of the ARGONAUTE4 (AGO4) clade and subsequently elicit *de novo* DNA methylation at target loci, such as transposable elements or protein-coding genes, through the RNA-directed DNA Methylation (RdDM) pathway **(25–29)**. Similar mechanisms could be utilized by *Smi* and *Smi2*; nevertheless, empirical tests to validate this hypothesis are missing.

In Brassica, the dominance hierarchy of *S*-alleles is proposed to rely on the combinatorial effect of single nucleotide variants at the *Smi* and *Smi2* sequences and at their respective *SCR* target sites **(8)**. In Arabidopsis, where more dominance classes exist, the dominance network is hypothesized to rely on two properties: i) recessive alleles carry more target sites and these sites are more generalist (*i.e.* they are targeted by more sRNA precursors than dominant alleles); and ii) sRNA precursors of dominant alleles are more generalist (*i.e.* they target a higher number of alleles than sRNA precursors in less dominant alleles) **(6)**. Despite this observation, the molecular features allowing sRNA precursors to target multiple alleles remain to be identified. In addition, among the eight families of sRNA precursors previously predicted to control the hierarchy in Arabidopsis, only one has been subject to formal experimental validation.

In this study, we aimed at identifying the molecular pathway underlying the sRNA-mediated dominance interactions between *S*-alleles in Arabidopsis. To achieve this, we engineered and characterized a series of *A. thaliana* lines recapitulating the self-incompatibility phenotype, and used these lines to show that two different sRNA precursors from dominant *A. halleri S*-loci trigger a decrease in abundance of recessive *SCR* transcripts. We thus provide a proof of concept that this heterologous approach can be used to validate sRNA precursor function, both at the phenotypic and at the molecular level. This system also allowed us to investigate if key components of the canonical RdDM pathway, such as the ARGONAUTE proteins AGO4 and AGO6, and subunits of the DNA-dependent RNA polymerases POLIV and POLV, are required for the repression of *SCR* transcript by *S*-locus sRNA precursors, and our analyses suggest that the two selected sRNA precursors do not act through the canonical RdDM pathway.

Additionally, and in order to better understand the role of sRNA precursors genes in the extensive and complex *S*-locus dominance network, we characterized their molecular features, revealing that despite their structural similarity to miRNAs genes, they rather resemble their evolutionary precursors: proto-miRNAs **(30, 31)**. Proto-miRNAs loci are inverted repeats present in several plant genomes that have acquired transcriptional competence, forming long hairpins which can be diced by multiple Dicer-like proteins (DCLs), leading to a complex population of sRNAs. There is little evidence that such a sRNA population could cause substantial effects in gene expression, at least through the canonical PTGS pathway **(32–36)**; therefore, these structures have been mostly regarded as substrates for selection to act on, rather than having immediate biological significance. Notwithstanding, we show that

S-locus proto-miRNA genes are able to influence the transcript abundance of *SCR* alleles, affect the pollen germination rate and, consequently, mediate *S*-allele dominance interactions. *S*-locus proto-miRNAs produce a large population of sRNAs with different sizes and sequences, which are important to maximize the number of targeted alleles, thus allowing one allele to be dominant over many others. Overall, our results provide a unique window into the function and evolution of proto-miRNAs, constituting the first example of a biological system that depends on their action.

Results

The sRNA precursors genes Ah04mir1887 and Ah20mirS3 control dominance interactions at the S-locus by decreasing the transcript level of the recessive SCR01 allele

To study in detail the molecular mechanisms controlling the activity of dominance modifiers in the self-incompatibility system of *A. halleri*, we first recreated the self-incompatibility reaction of *A. halleri* in the selfing species *A. thaliana*, since the latter is a more tractable study model. To do this, we expressed the *SRK01* receptor and its cognate *SCR01* ligand in female and male parents, respectively **(6, 37, 38)**. Manual crosses between these plants revealed that the germination of pollen from a fully fertile *SCR01*-expressing male was abolished when deposited on pistils of an *SRK01*-expressing female, the hallmark of a successful self-incompatible reaction **(Fig. 1C and D, wt panels)**. Given the challenges faced in prior studies to reconstruct this reaction in the Col-0 ecotype, all *A. thaliana* plants used in this study are of the C24 ecotype, where the self-incompatibility can be faithfully recreated as shown both in this, and other studies **(37, 39, 40)**.

Among the eight known families of *A. halleri* sRNA precursors loci, only one - mirS3 - has been experimentally validated to regulate dominance between two distinct *S*-alleles: specifically, the dominance of allele Ah20 over Ah01, mediated by Ah20mirS3 sRNAs, which target the *SCR01* intronic region **(Fig. 1B) (6)**. In this study, we set out to examine if the yet uncharacterized mir1887 family could have a similar function. For this, we focused on testing the role of the sRNA precursor Ah04mir1887 in controlling the dominance of allele Ah04 over Ah01, whose sRNAs are predicted to target the 5' region of *SCR01* **(Fig. 1A)**. We thus generated transgenic lines expressing Ah04mir1887 and introgressed this transgene into an *SCR01*-expressing male, and used these plants to pollinate *SRK01*-expressing females, testing whether the presence of the Ah04mir1887 sRNA precursor locus could transform the previously incompatible interaction between *SCR01* and *SRK01* into a compatible one **(Fig. 1C)**. In the particular case of Ah20mirS3, the transgenic line previously generated by Durand et al. **(6)** and used here expresses both Ah20mirS3 and Ah20mir1887 because of their close physical proximity within the Ah20 allele **(Fig. 1B)**. To specifically isolate the impact of Ah20mirS3 in the dominance interaction of Ah20 over Ah01, we developed the *SCR01*^{*mir1887} transgenic line, which contains five point mutations designed to fully disrupt the slight homology observed between some Ah20mir1887 sRNAs and *SCR01* **(Fig. 1B; Fig. 1 S1)**. We then used this modified *SCR01* line for all subsequent tests on the functional role of Ah20mirS3.

We observed that combining either Ah04mir1887 (Interaction A), or Ah20mirS3 (Interaction B) with *SCR01* results in a switch from an incompatible to a compatible pollen germination phenotype, which is accompanied by a dramatic decrease in the abundance of the *SCR01* transcript, as measured by

RT-qPCR **(Fig. 1C and D, wt panels)**. This shows that both Ah04mir1887 and Ah20mirS3 act as dominance modifiers in their respective allelic interactions, and that they accomplish this by decreasing *SCR01* transcript abundance, thus preventing SRK-SCR cognate recognition and allowing pollen germination to occur. Moreover, these results demonstrate that in Arabidopsis, *SCR* transcript abundance can be modulated by multiple sRNA precursor families that use distinct target sites in the *SCR* locus.

Decrease in SCR01 transcript abundance does not depend on RdDM

Next, we aimed at elucidating the exact molecular mechanism responsible for the reduction of *SCR01* transcript abundance triggered by the two *S*-locus sRNA precursors. Given their resemblance to miRNAs genes, one potential scenario is that sRNAs produced by Ah04mir1887 and Ah20mirS3 could trigger post-transcriptional gene silencing (PTGS) of the *SCR01* transcript. However, since these sRNAs are predicted to target the 5' region and intronic region of *SCR01*, and since the substrate of PTGS is generally thought to be the mature mRNA **(41)**, this does not support PTGS as the pathway responsible for the decrease in *SCR01* transcript abundance. An alternative scenario is that Ah04mir1887 and Ah20mirS3 sRNAs could trigger the RNA-directed DNA methylation pathway (RdDM), resulting in the deposition of DNA methylation in their respective *SCR01* target sites, and reduced *SCR01* transcription. Interestingly, previous studies have established that the silencing of recessive alleles in the homologous self-incompatibility system of *Brassica* relies on sRNA-mediated DNA methylation, although the specific pathway underlying this process remains elusive **(7, 8, 20)**. Thus, we focused our attention on the RdDM pathway, and set out to test if mutating key components of this pathway would prevent Ah04mir1887 and Ah20mirS3 from reducing *SCR01* transcript abundance. To circumvent the absence of RdDM mutant alleles in the C24 ecotype, we generated and validated C24 *ago4 ago6* CRISPR/Cas9 mutant alleles **(Fig. 1 S2)**, and used the previously published C24 *polIV* and *polV* knock-out alleles **(42)**.

To our surprise, none of the RdDM mutants impaired the activity of the tested sRNA precursors. In the case of Ah04mir1887, *SCR01* transcript abundance is reduced in all mutant backgrounds to a similar level as in wild-type, which is reflected by a compatible pollen germination phenotype **(Fig 1C)**. Similarly, the presence of Ah20mirS3 is associated with a decrease in *SCR01* transcript in all mutant backgrounds, showing that this sRNA precursor is still functional **(Fig. 1D)**. Remarkably, this is not reflected in a compatible pollen germination phenotype since the basal *SCR01* transcript level is increased in both *polIV* and *polV* mutant backgrounds when compared with wild-type **(Fig. 1D, *polIV* and *polV* panels vs. wt panel)**, pointing to an effect of these mutants on the expression of the *SCR01* transgene. This suggests that the *SCR01*^{*mir1887} construct might be intrinsically targeted for repression by RdDM, a phenomenon often observed in transgenic lines **(43)** (note that the *SCR01* and *SCR01*^{*mir1887} transgenes used in Interaction A and B, respectively, correspond to two independent transgenic lines with different insertion sites; **see Methods section**). As such, and even though the addition of Ah20mirS3 in these mutant backgrounds strongly reduces *SCR01* transcript abundance, it does not do so sufficiently to compromise the self-incompatibility reaction. Indeed, our data shows that

a strong reduction of *SCR01* transcript abundance is required for a compatible pollen germination phenotype, since even very low levels of transcript can trigger an incompatibility reaction **(Fig. 1 S3)**.

To further assess if the decrease in *SCR01* transcript abundance triggered by sRNA precursors is associated with deposition of DNA methylation at *SCR01* target sites, we used the BiSulfite Amplicon Sequencing technique - BSAS **(28, 44)**, which relies on PCR enrichment of regions of interest using bisulfite converted DNA as a template. *SCR01* expression is restricted to the tapetum cells of immature floral buds, which are challenging to manually isolate in *A. thaliana* due to their small size and embedment within other floral tissues. To overcome this limitation, we performed BSAS on 8-10 biological replicates of *SCR01* transgenic lines both in the presence and absence of the sRNA precursor transgenes **(Fig. 1 S4),** and generated an average coverage of 1400x for each cytosine located in the *SCR01* target sites and in the 800 bp around them **(Table S3)**. This allows us to detect minute DNA methylation differences between samples, thus compensating for the difficulty in enriching for tapetum tissue. We observed strong DNA methylation levels at the *SCR01* target sites **(Fig. 1 S4)**; however, no significant changes were detected in the presence of Ah04mir1887 or Ah20mirS3, suggesting that the decrease in *SCR01* transcript abundance is not mediated by changes in DNA methylation at the target sites **(Fig. 1 S4)**, which is in line with the absence of effects in the tested RdDM mutants. The observed high methylation levels at *SCR01* target sites, coupled with the specific *SCR01* expression in tapetum cells, led us to hypothesize that these methylation levels might represent the methylation status of surrounding floral tissues rather than specifically reflecting tapetum methylation. To investigate this further, we categorized BSAS reads based on the fraction of methylated cytosines within a single read. Our analysis revealed that a significant proportion of reads exhibited complete methylation, with a notable fraction showing little to no methylation **(Fig. 1 S5)**. We postulate that this subset of unmethylated reads may originate from tapetum cell DNA, where *SCR01* is actively expressed. Notwithstanding, no significant changes in unmethylated read abundance were detected in the presence of Ah04mir1887 or Ah20mirS3, again suggesting these sRNA precursors have no impact on DNA methylation.

Together, these results indicate that neither PTGS nor RdDM, at least in their canonical forms, appear to be responsible for the reduction in *SCR01* transcript abundance triggered by *S*-locus sRNA precursors. Despite this, both Ah04mir1887 and Ah20mirS3 strongly and robustly decrease *SCR01* transcript levels, which we show is necessary to abolish the self-incompatibility reaction.

Ah04mir1887 and Ah20mirS3 loci strongly resemble proto-miRNAs genes

S-locus sRNA precursors, including those of the mir1887 and mirS3 families studied here, consist of inverted repeats that are transcribed and predicted to form a RNA hairpin structures containing a 5' arm, a terminal loop and a complementary 3' arm **(Fig. 2A) (6)**, akin to the structures formed by precursor miRNA (pri-miRNA) molecules. To delve deeper into the molecular properties of Ah04mir1887 and Ah20mirS3, and to explore potential non-canonical pathways through which these precursors may act, we conducted sRNA sequencing on *A. thaliana* plants harboring the Ah04mir1887 and Ah20mirS3 transgenes. We observed that dicing of *S*-locus sRNA precursor hairpins leads to numerous sRNAs – at least 106 in the case of Ah04mir867, and 224 in the case of Ah20mirS3 **(Fig.**

2B-D). These sRNAs range from 18 to 25 nt in length, with no clear predominance of a specific length **(Fig. 2 S1 A-B)**, and their abundances vary by several orders of magnitude **(Fig. 2B, Fig. 2 S1 C-D)**.

Given the large population of sRNAs produced by a single precursor, we aimed at evaluating the functional relevance of each sRNA in controlling the abundance of the *SCR01* transcript. For this, we used a previously published algorithm **(6)**, which attributes a targeting score based on the homology between a single sRNA and the *SCR* genomic region. A previous study has demonstrated that in multiple *A. halleri S*-locus heterozygotes, a targeting score equal to or above 18 is associated with phenotypic dominance and a sharp decrease of the recessive *SCR* transcript level **(18)**. Using this algorithm, we found that 12 out of the total 106 sRNAs produced by Ah04mir1887, and 33 out of the total 224 sRNAs produced by Ah20mirS3, have a base-pairing score of ≥ 18 and are thus predicted to target *SCR01*. This subset of putatively functional sRNAs displays a variety of sizes and expression levels **(Fig. 2B, see grey box)**.

We additionally performed ARGONAUTE immunoprecipitation (IP) assays, followed by sRNA sequencing in the Ah04mir1887 and Ah20mirS3 *A. thaliana* transgenic lines, which showed that functional sRNAs produced from either precursor can be loaded into AGO1 (characteristic of the PTGS pathway) and AGO4 (characteristic of the RdDM pathway) **(Fig. 2 C-D)**. Notwithstanding this, a large part of these functional sRNAs (75% in Ah04mir1887 and 48% in Ah20mirS3) are not found to be loaded in either of these two AGO proteins, again consistent with our observations that both the canonical PTGS and RdDM pathways are unlikely to underlie the activity of these sRNA precursors. We also noted that the majority of sRNAs loaded in AGO1 have a 5' terminal uracil, reflecting the known AGO1 preference for binding these sRNAs **(45)**. However, sRNAs loaded into AGO4, or with an unknown loading pattern, do not show a significant bias towards a specific 5' nucleotide **(Fig. 2 S1 E-F)**. Overall, these results show that the predicted functionality of a given sRNA does not seem to be tied to a specific set of molecular features.

Despite the structural similarity between *S*-locus sRNA precursors and miRNAs, and the existence of shared features, such as the presence of mature 21-nt sRNAs and loading of sRNAs into AGO1, it is evident that *S*-locus sRNA precursors deviate from the typical characteristics associated with canonical miRNAs, and cannot be characterized as such. Instead, our data show that Ah04mir1887 and Ah20mirS3 highly resemble proto-miRNAs, the evolutionary predecessors of miRNAs: they have an unusually staggered hairpin processing pattern with numerous sRNAs derived from both the 5' and 3' arms, and differ in size, abundance and association with AGO proteins. Proto-miRNAs are thought to have no target genes and/or to cause no significant effect in transcript abundance **(30, 31, 33–36)**. This is not the case for Ah04mir1887 and Ah20mirsS3 since their effect on *SCR01* transcript levels is evident and necessary to modulate the self-incompatibility phenotype **(Fig. 1C and D, wt panels)**.

proto-miRNA features allow S-locus sRNA precursors to target multiple S alleles

We hypothesized that this heterogeneity in hairpin processing pattern could play an important role in the context of the complex *S*-locus dominance hierarchy by allowing a single sRNA precursor to exert dominance over multiple other alleles. To test this, we expanded our analysis of the function of

Ah04mir1887 and Ah20mirS3 beyond the interaction with allele Ah01, and looked at their role within the *A. halleri* dominance network **(Fig. 3)**.

We compiled previously published phenotypic data obtained by controlled reciprocal crosses between different *A. halleri S*-locus heterozygotes to determine the position of allele Ah20 and Ah04 in the dominance hierarchy of a total of 15 *S*-alleles **(Fig. 3) (6, 18, 46)**. From this, we could infer that Ah20 is dominant over 13 other *S*-alleles, with 10 of these interactions relying on the action of Ah20mirS3 **(Fig. 3)**, as determined by the sRNA-*SCR* targeting algorithm described above. Thus, Ah20mirS3 is not only able to mediate the repression of *SCR01*, but also the repression of at least nine other distinct *SCR* alleles. Similarly, Ah04mir1887 mediates the repression of at least five different *SCR* alleles that are recessive to Ah04 **(Fig. 3)**.

To test if the large population of sRNAs produced by these *S*-locus precursors is important in repressing multiple target alleles, we examined the role of each individual sRNA produced by both Ah04mir1887 and Ah20mirS3 **(Fig. 4)**: 11% of Ah04mir1887 sRNAs **(Fig. 4A, cluster 1)**, and 26% of Ah20mirS3 sRNAs **(Fig. 4B, cluster 1)** are predicted to target at least one *SCR* allele within the inferred dominance network presented in **Figure 3**. As is the case in Interaction A and B, there does not seem to be a clear correlation between abundance and sRNA functionality in any of the analyzed interactions **(Fig. 2B and Fig. 4A-B, see cluster 1 vs. cluster 2)**. Nevertheless, sRNAs that are predicted to be functional have a larger size than those that are not (median of 23 nt vs. 21 nt), and in the case of Ah20mirS3, this is also associated with a larger number of sRNAs being loaded in AGO proteins **(Fig. 4A-B; see cluster 1 vs. cluster 2).** Additionally, we can observe that most *S*-alleles are redundantly targeted by multiple sRNAs **(Fig. 4)**.

When investigating in more detail the positional correspondence between sRNAs and the Ah04mir1887/Ah20mirS3 precursor hairpin structure we noticed that sRNAs are produced in similar amounts from both the 5' and the 3' arms of the hairpin **(Fig. 5)**. Each hairpin arm produces numerous sRNAs that show a staggered pattern, suggesting imprecise dicing and resulting in a population of sRNAs that show small base-pair differences between them. In the case of Ah04mir1887, only the sRNAs produced from the 5' hairpin arm are predicted to be functional against the *S*-alleles tested here **(Fig. 5A)**. Remarkably, in the case of Ah20mirS3, each hairpin arm shows functional specialization since sRNAs from the 5' arm target all allele classes, except Class IV; while sRNAs from the 3' arm exclusively target Class IV and Class III alleles. Together, these observations suggest that the high number and heterogeneous processing of sRNAs is a conserved and important feature of *S*-locus sRNA precursors which allows targeting of multiple alleles and thus underlies their generalism.

Discussion

S-locus sRNA precursors act through non-canonical gene silencing pathways

Our characterization of self-incompatibility transgenic lines of *A. thaliana* contributes additional evidence to the work of Durand et al. **(6)**: collectively, these studies establish *A. thaliana* as a tractable system to study dominance interactions among *A. halleri S*-alleles and validate the role of two distinct sRNA precursor families in these interactions, yet the precise mechanisms underlying their action remain elusive. Our study reveals that some of the sRNAs generated in the processing of the *S*-locus

sRNA precursors have a length of 24 nt and are loaded into AGO4, potentially indicating a role for RdDM. Nevertheless, *ago4 ago6*, *polIV* and *polV* mutations did not significantly affect the action of *A. halleri S*-locus sRNA precursors, suggesting that canonical RdDM is not the primary mechanism through which Ah20mirS3 and Ah04mir1887 mediate the reduction in *SCR01* transcript levels. Considering their hairpin structure and their ability to also generate AGO1-loaded 21-nt sRNAs, it could also be envisioned that these precursors might act through PTGS. Still, the location of target sites in the 5' region and intronic regions of *SCR01* poses a conundrum, since PTGS is reported to occur in the cytoplasm, using mature mRNA as a cleavage substrate **(41)**. Notably, in animals, several lines of evidence point to miRNAs acting both in the cytoplasm and in the nucleus, with effects at the transcriptional and post-transcriptional levels **(47–49)**. In plants, it has been observed that an inverted repeat targeting the intron of the soybean gene *FAD12-1A* triggers cleavage of its precursor mRNA (pre-mRNA) in the nucleus, which is accompanied by accumulation of siRNAs of the cleaved pre-mRNA **(50)**. Additionally, all main miRNA processing components, including AGO1, are present in the nucleus **(51–53)**. Thus, given the independent slicer activity of AGO1 **(54)**, it could be hypothesized that this ARGONAUTE uses sRNAs to target the *SCR01* pre-mRNA in the nucleus, promoting its cleavage co-transcriptionally. Alternatively, the interaction between AGO1 and the *SCR* pre-mRNA could promote disassembly of the Poll II complex leading to the arrest of transcription, as has been suggested to occur in some miRNA genes upon salt stress **(55)**. Even though we could not detect any siRNAs corresponding to the cleavage of the *SCR01* pre-mRNA in any of our sRNA sequencing experiments **(data not shown)**, future experiments should investigate the possibility that the sRNA precursors at the *S*-locus could act through nuclear PTGS or through transcriptional arrest.

Our results that Ah20mirS3 and Ah04mir1887 work through an RdDM-independent pathway contrast with previous observations in Brassica: in this latter system, the sRNA precursors *Smi* and *Smi2* are associated with deposition of DNA methylation at *SCR* target sites and a decrease in *SCR* expression **(7, 8, 20)**. DNA methylation may result directly from the incorporation of *Smi* and *Smi2* sRNAs into AGO4-clade proteins, activating RdDM. Alternatively, as suggested by Finnegan et al. **(56)**, it could depend on *Smi*-induced cleavage of an antisense transcript at the *SCR* locus, generating sRNAs that could subsequently be co-opted into the RdDM pathway. Even though empirical investigations are still necessary to test these hypotheses, the cumulative evidence from these and our study suggests that different sRNA precursors within the Brassicaceae self-incompatibility system can elicit distinct effector pathways, that nevertheless converge into the same molecular phenotype: reduction of *SCR* transcript abundance. This would imply that these gene regulatory elements have an outstanding molecular flexibility, despite functioning within the specific evolutionary constraints of the self-incompatibility system. Thus, it cannot be excluded that different *A. halleri* sRNA precursors, as well as precursors from other self-incompatibility species such as *A. lyrata* and *Capsella grandiflora* could co-opt different gene regulatory pathways. Future investigations in these different species, using heterologous expression systems as done in this study, or in the native context whenever genetic transformation is feasible, will hopefully answer this outstanding question.

The complex S-allele dominance network relies on the unique features of S-locus sRNA precursors

Durand et al. **(6)** previously showed that the *S*-locus sRNA precursors of *A. halleri* have high generalism, and suggested that dominant *S*-alleles in particular, rely on this ability to target multiple recessive alleles, rather than on carrying an increased number of sRNA precursors. Our study uncovers the molecular basis for this generalism, and shows that the apparent haphazardous processing of *S*-locus sRNA precursors is required to generate numerous functional sRNAs that target multiple alleles cooperatively: remarkably, all *SCR* alleles analyzed in this study are targeted by multiple sRNAs of a single sRNA precursor, and/or are targeted by distinct sRNA precursors. This contrasts with the less complex dominance hierarchy of Brassica, where fewer allelic interactions are present, and a single functional sRNA molecule *per* precursor has been suggested to mediate all dominance relationships **(7, 8)**. It is important to note that while we investigated a total of 15 *S*-alleles in this study, at least 43 are known to exist in *A. halleri* **(15)**, and > 80 in the closely related *Capsella grandiflora* **(22)**. Therefore, in this study we most likely underestimated the fraction of functional sRNAs in each precursor, since those that are non-functional in the allelic interactions explored here could potentially have a role in interactions that have not yet been characterized.

Overall, the evidence suggests that collaborative targeting, either by multiple sRNAs of a single precursor, or by sRNAs from distinct sRNA precursors, is an essential feature of this system: firstly, it is essential for granting an *S*-allele its complete targeting spectrum across the many *S*-alleles segregating in the population; and secondly, the use of multiple sRNAs with distinct molecular features could trigger diverse effector pathways acting on the same target allele, which could perhaps underlie the robust reduction of recessive *SCR* transcripts observed in all allelic interactions studied thus far (this study and **(18)**).

Intriguingly, this mirrors the collaborative non-self recognition model observed in Solanaceae, where each self-incompatibility allele contains multiple *SLF* genes. SLF proteins play a crucial role in recognizing and removing the toxic non-self female S-RNase, which otherwise inhibits pollen germination. In this system, the presence of multiple *SLF* genes within a single S-locus allele, each capable of recognizing a distinct S-RNase allele, coupled with the ability of some *SLF* genes to recognize and detoxify multiple S-RNases (generalism), is crucial. This collaborative functionality among *SLF* genes ensures a comprehensive recognition spectrum for a given self-incompatibility allele, thereby preserving the intricate inter-allelic interaction network within Solanaceae **(57)**. While in Solanaceae, the generalism of SLF proteins likely depends on their ability to establish protein-protein interactions with distinct S-RNases **(58)**, in *A. halleri*, sRNA precursor generalism relies on their unique molecular features, specifically their ability to produce numerous sRNAs with distinct targeting spectra.

S-locus sRNA precursors provide a window into the miRNA evolution continuum

Although sharing some structural similarities with miRNAs, the features of *S*-locus sRNA precursors more closely resemble those of proto-miRNAs. We hypothesize that the specific selective constraints of the *S*-locus dominance network have likely contributed to the persistence of proto-miRNA features over extended evolutionary times, and prevented their progression towards canonical miRNA features, as this would likely render them unable to effectively target multiple *S*-alleles. It would be interesting to

test if apparently stabilized proto-miRNAs are also used in other biological systems where the expression of multiple genes/alleles needs to be coordinated by a single regulator and under similar evolutionary constraints as those acting on the *S*-locus. The mimicry of wing patterns in *Heliconius* butterflies would be an interesting model system to test this, since balancing selection has favored the appearance of numerous alleles of the supergene controlling wing pattern, and dominance relationships between them are prevalent **(59, 60)**.

To our knowledge, the *A. halleri S*-locus sRNA precursors represent the first instance where proto-miRNA-like features are biologically relevant, and actively selected for. And despite not conforming to canonical gene regulatory pathways, our data shows that *S*-locus proto-miRNAs exert a considerable impact on gene expression. Prior investigations of proto-miRNA function have primarily evaluated the functionality of these structures in the light of canonical miRNA pathways, often concluding that their functional impact is negligible **(32–36)**. Based on our findings, we propose that further exploration is necessary to determine whether proto-miRNAs can employ non-canonical pathways to regulate gene expression in diverse biological contexts beyond the *S*-locus. Investigating the function and mode of action of proto-miRNAs in different organisms will contribute not only to better understand their potential roles, but also to uncover the key steps in the emergence of proto-miRNAs and their transition into canonical miRNAs.

Materials and Methods

Plant material & growing conditions

Wild-type (wt) and transgenic *Arabidopsis thaliana* plants used in this study were grown in a greenhouse, using standard growth conditions (16 h light/8 h dark; 110 µmol/s/m2; 21°C; 70% humidity). Seeds were germinated directly on soil, or in MS-medium (0.43% MS-salts, 0.8% Bacto agar, 0.19% MES hydrate, and 1% sucrose) when antibiotic selection was necessary for transgene selection.

Because the self-incompatibility reaction cannot be faithfully reconstructed in the *A. thaliana* Col-0 ecotype **(37–40)** all wild-type and mutant plants used in this study were of the C24 ecotype. *polIV* and *polV* correspond to the previously published and validated *rdm5 (nrpd1a)* and *rdm6 (nrpd1b*) mutant alleles **(42)**. These two mutants were generated in the *ros1* mutant background, which was removed in our study by backcrossing to wt C24 plants. The *ago4 ago6* double mutant was generated in the C24 background using CRISPR/Cas9 **(see section *Generation and validation of CRISPR/Cas9 mutants* for more details)**.

To obtain the *S*-allele sequences of Ah65, Ah60, Ah03, Ah33 and Ah19, five *Arabidopsis halleri* individuals containing a combination of these alleles were collected from diverse natural European populations **(61)**, and grown under standard greenhouse conditions in order to obtain plant material for DNA extraction and sequencing **(see the section *DNA extraction, Nanopore sequencing and assembly of S-alleles* for more details)**. Following Goubet et al. **(23)**, we further obtained the S-allele sequence of Ah01, Ah02 and Ah25 by constructing and screening BAC libraries from fresh leaf samples, and fully sequencing the positive clones using PACBIO.

Cloning

Several transgenic lines were used in this study: lines carrying SRK01, SCR01, and the sRNA precursor Ah20mirS3 were cloned as detailed previously **(6)**.

The precursors Ah20mir1887 and Ah20mirS3 are in very close physical proximity within the Ah20 allele, and the previously published Ah20mirS3 line contains both sRNA precursors **(6)**. While performing sRNA sequencing of AGO-IP experiments **(see section *ARGONAUTE immunoprecipitation and sRNA sequencing*)**, we noticed that some Ah20mir1887 sRNAs show homology to the 5' region of *SCR01*. The base-pairing score of these predicted interactions varies between 12.5 and 18.5, depending on the sRNAs **(Fig. 1 S1, see the section *Target site inference for Ah04mir1887 and Ah20mirS3* for more details on these scores)**. To confidently isolate the effect of Ah20mirS3 in the dominance interaction of Ah20 over Ah01 (Interaction B), we introduced five point mutations in the SCR01^{*mir1887} sequence that disrupt the homology with the Ah20mir1887 sRNAs, rendering the Ah20mir1887 target site non-functional. The SCR01^{*mir1887} transgene was generated by performing site-directed mutagenesis on the already published SCR01 clone **(6)**, using the primers detailed in **table S1**. The resulting amplicon was then recombined into the entry vector pDONR-Zeo, and subsequently recombined into the pB7m34GW destination vector using the 3-fragment Gateway Cloning System (Invitrogen), including 5' and 3' mock sequences, as detailed previously **(6)**.

Ah04mir1887 was cloned by amplifying a region spanning this sRNAs precursor and containing 2 kb of upstream and downstream sequences from a BAC clone carrying allele Ah04, using the primers detailed in **table S1**. The resulting amplicon was then recombined into the entry vector pDONR-Zeo, and subsequently recombined into the pH7m34GW destination vector using the 3-fragment Gateway Cloning System (Invitrogen), including 5' and 3' mock sequences, as detailed previously **(6)**.

Arabidopsis thaliana C24 plants were transformed using the floral dip method **(62)**, and transgenic lines were selected using the appropriate antibiotics.

Generation and validation of CRISPR/Cas9 mutants

Given the aforementioned limitation that the self-incompatibility reaction of *A. halleri* can only be reconstituted in the *A. thaliana* C24 ecotype **(37–40)**, we created the *ago4 ago6* RdDM mutants in this specific ecotype using CRISPR/Cas9. The expression cassette of pCBC-DT1T2 **(63)** was amplified using two overlapping forward and reverse primers that contained two gene-specific sgRNA sequences (Fw1: 5'-ATATATGGTCTCGATTGNNNNNNNNNNNNNNNNNNGTT-3'; Fw2: 5'-TGNNNNNNNNNNNNNNNNNNGTTTTAGAGCTAGAAATAGC-3'; Rv1: 5'-ATTATTGGTCTCGAAACNNNNNNNNNNNNNNNNNNCAA-3'; Rv2: 5'-AACNNNNNNNNNNNNNNNNNNCAATCTCTTAGTCGACTCTAC-3', where N corresponds to the gene-specific gRNAs **(table S1)**, and underlined regions correspond to BsaI restriction sites). The amplicons obtained from this PCR reaction were gel-isolated and inserted into pHEE401E **(64)** using BsaI and T4 ligase (Thermo Fisher Scientific). The pHEE401E vectors containing gRNAs against *AGO4* and *AGO6* were transformed into the *Agrobacterium tumefaciens* strain GV3101. The floral-dip method **(62)** was then used to transform wt C24 *A. thaliana* plants.

To screen for T1 mutant plants, the regions targeted by the gRNAs were Sanger sequenced to identify *ago4 ago6* mutants with premature stop codons in both genes **(Fig. 1 S2)**. In the T2 generation, double homozygous mutants that did not carry the pHEE401E were selected by genotyping **(see table 1 for primers)**.

To confirm that *ago4 ago6* mutations impair DNA methylation, a Chop-PCR assay was performed **(65)**. Briefly, this assay uses genomic DNA treated with the methylation-sensitive enzyme HaeIII as a template for PCR. Primers targeting regions known to have AGO4/AGO6-dependent DNA methylation, as well as control unmethylated regions are amplified **(see table S1 for primers)**. Using this method, we could determine that the *ago4 ago6* mutant generated in this study shows reduced DNA methylation levels, as has been previously published for other mutant alleles of these genes **(Fig. 1 S2 C) (66)**.

Pollen germination assays

All lines used for the reconstruction of the self-incompatibility reaction in *A. thaliana* were used in hemizygous state to mimic the abundance of sRNA precursors, and *SCR/SRK* in *A. halleri* individuals heterozygous at the *S*-locus. Genotyping of each transgenic line/mutant was done by classical PCR, or using the KASPar assay **(67) (table S1)**. Paternal plants hemizygous for *SCR01* and sRNA precursors were obtained by crossing *SCR01* to Ah04mir1887 homozygous lines or by crossing *SCR01*^{*mir1887} to Ah20mirS3 homozygous lines.

To assess the self-incompatibility reaction at the phenotypic level, pollen germination assays were performed on manually crossed plants. Maternal plants hemizygous for *SRK01* were emasculated one day before anthesis, and manually pollinated 24h later with paternal plants hemizygous for *SCR01,* *SCR01*^{*mir1887}, *SCR01* Ah04mir1887 or *SCR01*^{*mir1887} Ah20mirS3. Pollinated pistils were transferred to fixing solution 6h after pollination and stained with aniline blue, as described before **(6)**. These pistils were then mounted on microscope slides and imaged using a Zeiss AX10 fluorescence microscope, where we counted the number of germinated pollen grains present in each pistil.

To evaluate the effect of RdDM mutants on the activity of *S*-locus sRNA precursors we crossed the RdDM mutants *ago4 ago6*, *polIV* and *polV* with the previously described paternal plants carrying *SCR01* and sRNA precursors (*SCR01, SCR01*^{*mir1887}, *SCR01* Ah04mir1887 and *SCR01*^{*mir1887} Ah20mirS3). We then obtained plants hemizygous for the *SCR01* and sRNA precursor transgenes and homozygous for the mutations of interest and used these as paternal plants in crosses with maternal hemizygous *SRK01* plants, as described above.

As a control, all maternal and paternal lines used in this study were crossed to wt C24. Germination and seed set for all these genotypes were comparable to that of wt x wt crosses **(data not shown)**, confirming that the transgenes and mutations had no detectable effect on plant fertility.

RT-qPCR

To measure the abundance of *SCR01* transcripts, we isolated immature buds of plants hemizygous for *SCR01, SCR01*^{*mir1887}, *SCR01* Ah04mir1887 or *SCR01*^{*mir1887} Ah20mirS3. RNA was extracted using the NucleoSpin RNA Plus kit (Macherey-Nagel) and cDNA was synthesized with the RevertAid First Strand cDNA Synthesis Kit (Thermo Scientific). qPCR was performed using the iTaq Universal SYBR

Green Supermix (BioRad) in a Lightcycler 480 instrument (Roche), with the primers found in **table S1**. *ACT8* was used as a reference gene. Transcript abundance was quantified using the Pfaffl method **(68)**.

ARGONAUTE immunoprecipitation and sRNA sequencing

AGO1 and AGO4 immunoprecipitation (IP) assays were performed on immature buds of plants carrying a homozygous Ah04mir1887 or Ah20mirS3 transgenes, using a previously published protocol **(69)**, with the following modifications: IPs were performed on 1.4 g of finely ground powder of frozen immature buds. The anti-AGO1 (AS09 527, Agrisera) and anti-AGO4 (AS09 617, Agrisera) antibodies were added at a 1/500 dilution for the incubation step and their immobilization was performed using Dynabeads Protein G (Invitrogen). The IP products were washed six times with PBS prior to sRNA extraction using the Trizol reagent (Ambion). In parallel, an aliquot of each input extract was used for total sRNA isolation using the Trizol LS reagent (Invitrogen), according to the supplier instructions. For each genotype three sRNA fractions were obtained: AGO1-IP, AGO4-IP and input.

These three sRNA fractions were subjected to an acrylamide gel-based size selection for sRNAs. These sRNAs were then used for TruSeq Small RNA (Illumina) library preparation and sequenced on a NextSeq 500 platform (Illumina), using 75 bp single-reads. Reads were trimmed, quality filtered, and size-selected using TrimGalore **(70)**. We followed a two-step mapping procedure with ShortStack (allowing for one mismatch) **(71)**, where we mapped sRNAs from each sample to the *A. thaliana* TAIR10 genome (masking the *S*-locus region), and to the sequence of the corresponding *A. halleri S*-allele (Ah04, for samples carrying Ah04mir1887 and Ah20 for samples carrying Ah20mirS3). Only reads that mapped exclusively to the *S*-locus were kept for further analysis. sRNA read counts were normalized to rpm to allow comparison of abundance levels across samples.

AGO loading was inferred based on the ratio of reads found in the AGO1-IP fraction and the AGO4-IP fraction: a sRNA was considered to be loaded in AGO1 or AGO4 when more than 50% of its total reads were derived from either the AGO1-IP fraction or the AGO4-IP fraction, respectively. A given sRNA was classified as having an unknown loading when no reads were found in both AGO-IP fractions, or when the amount of reads found in the input fraction was superior to that found in any of the two AGO-IP fractions.

Target site inference for Ah04mir1887 and Ah20mirS3

To identify sRNA target sites on *SCR* genomic regions, we first generated a database containing all sRNAs sequenced in the AGO-IP experiments described above. In parallel, a database containing *SCR* genomic regions of different *A. halleri S*-loci was compiled. This included alleles from all four dominance classes, and comprised previously published sequencing data **(see *Data Availability* section for a complete list of data sources)**. In addition to this, long read Nanopore sequences newly obtained from individuals carrying alleles Ah65, Ah60, Ah03, Ah33 and Ah19 were also added to this database **(see section *Nanopore sequencing and assembly of S-alleles* for more details)**.

Using the databases of sRNA sequences and *SCR* alleles, we applied a previously published homology detection algorithm **(6)** to find target sites. Functional sRNA are defined as those with a

533 homology score of ≥ 18, since this score has been consistently shown to be associated with a decrease
534 in *SCR* transcript abundance of the targeted allele (6, 18). The identified sRNA - *SCR* interactions were
535 then represented in a heatmap **(Fig. 4)** using ComplexHeatmap **(72)**, and in a circos plot **(Fig. 5)** using
536 circlize **(73)**.

537 *DNA extraction, Nanopore sequencing and assembly of S-alleles*

538 To obtain the *S*-locus sequences of alleles Ah65, Ah60, Ah03, Ah33 and Ah19, 2 g of fresh leaves
539 were collected from five different individuals carrying these alleles and flash-frozen. High molecular
540 weight genomic DNA was extracted as described before **(74)**. Long read sequences were obtained by
541 Oxford Nanopore Technologies (ONT) flowcells v9. To polish the contigs obtained by long read
542 sequencing Illumina data were also generated (with no step of PCR amplification to minimize
543 sequencing bias).

544 For Nanopore library preparation, the smallest genomic DNA fragments were first eliminated using
545 the Short Read Eliminator Kit (Pacific Biosciences). Libraries were then prepared according to the
546 protocol 1D Native barcoding genomic DNA (with EXP-NBD104 and SQK-LSK109) provided by Oxford
547 Nanopore Technologies. Depending on how many samples were pooled, 250 ng (pool of 9 samples) to
548 1 µg (pool of 4 samples) of genomic DNA fragments were repaired and end-prepped with the NEBNext
549 FFPE DNA Repair Mix and the NEBNext Ultra II End Repair/dA-Tailing Module (New England Biolabs).
550 Barcodes provided by ONT were then ligated using the Blunt/TA Ligase Master Mix (NEB). Barcoded
551 fragments were purified with AMPure XP beads (Beckmann Coulter), then pooled and ONT adapters
552 were added using the NEBNext Quick Ligation Module (NEB). After purification with AMPure XP beads
553 (Beckmann Coulter), each library was mixed with the sequencing buffer (ONT) and the loading beads
554 (ONT) and loaded on a PromethION R9.4.1 flow cell. In order to maintain the translocation speed, flow
555 cells were refueled with 250 µl Flush Buffer when necessary. Reads were basecalled using Guppy
556 version 3.2.10, 4.0.11, 5.0.12, 5.0.13, 5.0.16 or 5.1.12. The Nanopore long reads were not cleaned and
557 raw reads were used for genome assembly.

558 For Illumina PCR-free library preparation, 1.5 µg of genomic DNA was sonicated to a 100–1500-bp
559 size range using a Covaris E220 sonicator (Covaris). The fragments (1µg) were end-prepped, and
560 Illumina adapters (NEXTFLEX Unique Dual Index Barcodes, Perkin Elmer) were added using the Kapa
561 Hyper Prep Kit (Roche). The ligation products were purified twice with 1X AMPure XP beads (Beckman
562 Coulter). The libraries were then quantified by qPCR using the KAPA Library Quantification Kit for
563 Illumina Libraries (Roche), and their profiles were assessed on an Agilent Bioanalyzer (Agilent
564 Technologies). The libraries were sequenced on an Illumina NovaSeq 6000 instrument (Illumina) using
565 150 base-length read chemistry in a paired-end mode.

566 Nanopore sequencing data were assembled using Necat **(75)** with a genome size of 240 Mbp and
567 the remaining parameters left as default. Contigs produced by Necat were polished one time using
568 Racon **(76)** with Nanopore reads, then one time with Medaka
569 (https://github.com/nanoporetech/medaka, model r941_prom_hac_g507) and Nanopore reads, and two
570 times with Hapo-G v1.3.4 **(77)** and Illumina short reads. However, the cumulative sizes of our long-read
571 assemblies were larger than the estimated 240 Mb, suggesting that the assembly size was currently

572 inflated by the presence of allelic duplications. Thus, HaploMerger2 **(78)** was run (Batch A twice to
573 remove major misjoin and one Batch B) to generate a haploid version of each assembly.
574 To detect the *S*-locus region in the generated assemblies, blast searches were performed using the
575 genes flanking the *S*-locus (*ARK3* and *U-box* **(23)**) as queries. This allowed us to precisely narrow down
576 the genomic regions corresponding to the full Ah65, Ah60, Ah03, Ah33 and Ah19 *S*-alleles. We
577 annotated *SRK* using blast searches, and following Goubet et al. **(23)**, we used Fgenesh+ **(79)** to predict
578 the genomic sequence of *SCR* based on a database of SCR protein sequences from already known S-
579 alleles.

580 *Phenotypic determination of the S-loci dominance hierarchy*

581 The *S*-locus dominance hierarchy in **Fig. 3** is based on a compilation of controlled reciprocal crosses
582 between different *A. halleri* individuals **(6, 18, 46, 80)**. In cases where interactions between alleles of
583 two different dominance classes had not been tested phenotypically, dominance was inferred based on
584 the phylogenetic class of each allele, since interclass dominance interactions are predictable **(15, 24)**.
585 In the case of intraclass relationships, such as for alleles Ah65, Ah60 and Ah33 (all belonging to class
586 III), phenotypic dominance has not been determined yet, and thus the ordering of these alleles along
587 the hierarchy remains arbitrary at this stage.

588 *BSAS sequencing*

589 To measure DNA methylation in *SCR01* target sites we used the BiSulfite Amplicon Sequencing
590 Technique - BSAS **(28, 44)** which relies on PCR enrichment of regions of interest using bisulfite
591 converted DNA as a template. To assess if the presence of *S*-locus sRNA precursors is associated with
592 DNA methylation changes in the respective *SCR01* target regions, we isolated immature buds of
593 *SCR01, SCR01*^{*mir1887}, *SCR01* Ah04mir1887 and *SCR01*^{*mir1887} Ah20mirS3 plants. Genomic DNA was
594 extracted using the NucleoSpin Plant II kit (Macherey-Nagel), and converted with the EZ DNA
595 Methylation Kit (Zymo Research), including the modifications A and B, as described by the supplier, to
596 optimize the conversion efficiency. Eight to ten biological replicates were extracted and converted for
597 each genotype. Converted DNA was then amplified using primers flanking the Ah04mir1887 or
598 Ah20mirS3 target sites in the intron and 5' region regions of *SCR01*, respectively **(table S1)**. For each
599 sRNA precursor, seven amplicons were generated, which amplify the top and bottom strands of the
600 ~800 bp that flank the target site. As a negative control, we also amplified *AT2G20610*, which has been
601 previously described to be an unmethylated negative control in *A. thaliana* Col-0 plants **(28)**.
602 Amplification of bisulfite converted DNA was performed using the TaKaRa EpiTaqTM HS (Takara), and
603 the resulting PCR reactions were cleaned-up using the NucleoSpin Gel and PCR Clean-up XS kit
604 (Macherey-Nagel). All amplicons obtained from a single biological replicate were pooled in equimolar
605 amounts and a total of 100 ng were used for library preparation following the modified Illumina Nextera
606 Flex library preparation protocol described before (28, 81). Libraries were sequenced in a MiSeq
607 (Illumina) platform using 250 bp paired-end reads. Reads were trimmed, quality-filtered, and mapped
608 to the Ah01 allele using methlypy **(82)**, following the paired-end pipeline and specifying *AT2G20610* as
609 the unmethylated control. Conversion efficiencies for each sample were estimated based on the

methylation levels detected in the *AT2G20610* locus, and were between 97% and 83% **(table S2)**. The number of methylated reads covering each *SCR01* cytosine position, as outputted by methylpy, can be found in **table S3**. Average DNA methylation levels within the top and bottom strands of the ~800 bp regions flanking Ah04mir1887 and Ah20mirS3 target sites were summarized in R **(83)** and plotted with ggplot2 **(84)**.

To identify DNA methylation heterogeneity at the single-molecule level, the methylation rate over each single read aligned to the *SCR01* sequence in three different cytosine contexts (CG, CHG and CHH) was computed using the Bismark methylation call output **(85)**. For each sample, reads were classified in three distinct categories: highly methylated reads with 90% or more methylated cytosines, weakly methylated reads with a methylation rate inferior to 10%, and everything in between. Statistical differences in number of highly and weakly methylated reads between the *SCR01* and *SCR01* Ah04mir1887 or *SCR01*^{*mir1887} and *SCR01*^{*mir1887} Ah20mirS3 genotypes were assessed using a two-tailed Mann-Whitney test with continuity correction.

Data availability

The AGO-IP and sRNA sequencing data is deposited in the Gene Expression Omnibus database, under the SubSeries reference GSE249507.

The Illumina and Oxford Nanopore sequencing data of the five *A. halleri* individuals carrying alleles Ah65, Ah60, Ah03, Ah33 and Ah19 are available in the European Nucleotide Archive, under the project number PRJEB70880.

The *S*-locus sequences used in this study are a combination of previously published data (6, 23) and data generated in this study. All allele sequences can be found in GenBank, under the following references: Ah01 - this study, PP396894; Ah02 - this study, PP396895; Ah03 - this study, PP537897; Ah04 - KJ461484; Ah10 - KM592810 and KM592817; Ah12 - KJ772373 and KJ772377; Ah13 - KJ461479 and KJ461483; Ah19 - this study, PP537898; Ah20 - FO203486; Ah25 - this study, PP396896; Ah28 - KJ461478; Ah29 - KM592803; Ah33 - this study, PP537899; Ah60 - this study, PP537900; Ah65 - this study, PP537901.

Acknowledgments

This work was supported by a European Molecular Biology Organization (EMBO) Postdoctoral Fellowship attributed to RAB, by the European Research Council (NOVEL project, grant #648321) and by the French National Research Agency (TE-MoMa project, grant ANR-18-CE02-0020-01). This work was performed using the infrastructure and technical support of the Plateforme Serre, Cultures et Terrains Expérimentaux - Université de Lille for the greenhouse/field facilities. Research at the Lagrange laboratory was supported by the Centre National de la Recherche Scientifique (CNRS) and Université de Perpignan Via Domitia (UPVD). This study is set within the framework of the "Laboratoires d'Excellences (LABEX)" TULIP (ANR-10-LABX-41) and the "Ecole Universitaire de Recherche" (EUR) TULIP-GS (ANR-18-EURE-0019). Research at the Krämer laboratory was supported by the Deutsche Forschungsgemeinschaft DFG in SPP 1529 (ADAPTOMICS, Kr1967/10-1,-2), and by ERC-AdG LEAP-

EXTREME (788380). We thank Hervé Vaucheret, Vincent Colot, Claudia Köhler and Nicolas Butel for helpful discussions, and Hervé Vaucheret for sharing seeds.

References

1. Mendel, G., "Experiments on Plant Hybrids (Sherwood, E.R., trans.)" in *The Origin of Genetics: A Mendel Source Book (Stern, C. and Sherwood, E.R., Eds)*, (W.H. Freeman, 1865), pp. 1–48.
2. S. Billiard, V. Castric, V. Llaurens, The integrative biology of genetic dominance. *Biol. Rev.* **96**, 2925–2942 (2021).
3. S. Billiard, V. Castric, Evidence for Fisher's dominance theory: How many "special cases"? *Trends Genet.* **27**, 441–445 (2011).
4. R. A. Fisher, The Possible Modification of the Response of the Wild Type to Recurrent Mutations. *Am. Nat.* **62**, 115–126 (1928).
5. S. Wright, Physiological and Evolutionary Theories of Dominance. *Am. Nat.* **68**, 24–53 (1934).
6. E. Durand, *et al.*, Dominance hierarchy arising from the evolution of a complex small RNA regulatory network. *Science* **346**, 1200–1205 (2014).
7. Y. Tarutani, *et al.*, Trans-acting small RNA determines dominance relationships in Brassica self-incompatibility. *Nature* **466**, 983–986 (2010).
8. S. Yasuda, *et al.*, A complex dominance hierarchy is controlled by polymorphism of small RNAs and their targets. *Nat. Plants* **3**, 1–5 (2016).
9. J. Huang, *et al.*, Stigma receptors control intraspecies and interspecies barriers in Brassicaceae. *Nature* **614**, 303–308 (2023).
10. C. Liu, *et al.*, Pollen PCP-B peptides unlock a stigma peptide–receptor kinase gating mechanism for pollination. *Science* **372**, 171–175 (2021).
11. J. B. Nasrallah, Stop and go signals at the stigma–pollen interface of the Brassicaceae. *Plant Physiol.* kiad301 (2023). https://doi.org/10.1093/plphys/kiad301.
12. J. B. Nasrallah, "Self-incompatibility in the Brassicaceae: Regulation and mechanism of self-recognition" in *Current Topics in Developmental Biology*, (Academic Press, 2019), pp. 435–452.
13. L. Zhang, *et al.*, FERONIA receptor kinase-regulated reactive oxygen species mediate self-incompatibility in Brassica rapa. *Curr. Biol.* **31**, 3004-3016.e4 (2021).
14. V. Castric, J. Bechsgaard, M. H. Schierup, X. Vekemans, Repeated adaptive introgression at a gene under multiallelic balancing selection. *PLoS Genet.* **4** (2008).
15. M. Genete, V. Castric, X. Vekemans, Genotyping and De Novo Discovery of Allelic Variants at the Brassicaceae Self-Incompatibility Locus from Short-Read Sequencing Data. *Mol. Biol. Evol.* **37**, 1193–1201 (2020).
16. M. J. Lawrence, Population Genetics of the Homomorphic Self-incompatibility Polymorphisms in Flowering Plants. *Ann. Bot.* **85**, 221–226 (2000).
17. K. Sato, *et al.*, Coevolution of the S-Locus Genes SRK, SLG and SP11/SCR in Brassica oleracea and B. rapa. *Genetics* **162**, 931–940 (2002).
18. N. Burghgraeve, *et al.*, Base-Pairing Requirements for Small RNA-Mediated Gene Silencing of Recessive Self-Incompatibility Alleles in Arabidopsis halleri. *Genetics* **215**, genetics.303351.2020

(2020).

19. T. Kakizaki, *et al.*, Linear Dominance Relationship among Four Class-II S Haplotypes in Pollen is Determined by the Expression of SP11 in Brassica Self-Incompatibility. *Plant Cell Physiol.* **44**, 70–75 (2003).
20. H. Shiba, *et al.*, The Dominance of Alleles Controlling Self-Incompatibility in Brassica Pollen Is Regulated at the RNA Level. *Plant Cell* **14**, 491–504 (2002).
21. V. Llaurens, S. Billiard, V. Castric, X. Vekemans, Evolution of dominance in sporophytic self-incompatibility systems: I. genetic load and coevolution of levels of dominance in pollen and pistil. *Evolution* **63**, 2427–2437 (2009).
22. T. Duan, *et al.*, Dominance between self-incompatibility alleles determines the mating system of Capsella allopolyploids. [Preprint] (2023). Available at: https://www.biorxiv.org/content/10.1101/2023.04.17.537155v1 [Accessed 19 September 2023].
23. P. M. Goubet, *et al.*, Contrasted Patterns of Molecular Evolution in Dominant and Recessive Self-Incompatibility Haplotypes in Arabidopsis. *PLoS Genet.* **8**, e1002495 (2012).
24. N. L. Prigoda, A. Nassuth, B. K. Mable, Phenotypic and genotypic expression of self-incompatibility haplotypes in Arabidopsis lyrata suggests unique origin of alleles in different dominance classes. *Mol. Biol. Evol.* **22**, 1609–1620 (2005).
25. P. Chellappan, *et al.*, siRNAs from miRNA sites mediate DNA methylation of target genes. *Nucleic Acids Res.* **38**, 6883–6894 (2010).
26. B. Khraiwesh, *et al.*, Transcriptional Control of Gene Expression by MicroRNAs. *Cell* **140**, 111–122 (2010).
27. K. Panda, *et al.*, Full-length autonomous transposable elements are preferentially targeted by expression-dependent forms of RNA-directed DNA methylation. *Genome Biol.* **17**, 170 (2016).
28. M. J. Sigman, *et al.*, An siRNA-guided ARGONAUTE protein directs RNA polymerase V to initiate DNA methylation. *Nat. Plants* **7**, 1461–1474 (2021).
29. L. Wu, *et al.*, DNA Methylation Mediated by a MicroRNA Pathway. *Mol. Cell* **38**, 465–475 (2010).
30. E. Allen, *et al.*, Evolution of microRNA genes by inverted duplication of target gene sequences in Arabidopsis thaliana. *Nat. Genet.* **36**, 1282–1290 (2004).
31. M. J. Axtell, J. O. Westholm, E. C. Lai, Vive la différence: biogenesis and evolution of microRNAs in plants and animals. *Genome Biol.* **12**, 221 (2011).
32. J. Cui, C. You, X. Chen, The evolution of microRNAs in plants. *Curr. Opin. Plant Biol.* **35**, 61–67 (2017).
33. J. T. Cuperus, N. Fahlgren, J. C. Carrington, Evolution and Functional Diversification of MIRNA Genes. *Plant Cell* **23**, 431–442 (2011).
34. N. Fahlgren, *et al.*, Microrna gene evolution in Arabidopsis lyrata and Arabidopsis thaliana. *Plant Cell* **22**, 1074–1089 (2010).
35. N. Fahlgren, *et al.*, High-throughput sequencing of Arabidopsis microRNAs: Evidence for frequent birth and death of MIRNA genes. *PLoS ONE* **2**, e219 (2007).
36. R. Rajagopalan, H. Vaucheret, J. Trejo, D. P. Bartel, A diverse and evolutionarily fluid set of microRNAs in Arabidopsis thaliana. *Genes Dev.* **20**, 3407–3425 (2006).

37. M. E. Nasrallah, P. Liu, S. Sherman-Broyles, N. A. Boggs, J. B. Nasrallah, Natural variation in expression of self-incompatibility in Arabidopsis thaliana: Implications for the evolution of selfing. *Proc. Natl. Acad. Sci.* **101**, 16070–16074 (2004).
38. M. E. Nasrallah, P. Liu, J. B. Nasrallah, Generation of Self-Incompatible Arabidopsis thaliana by Transfer of Two S Locus Genes from A. lyrata. *Science* **297**, 247–249 (2002).
39. N. A. Boggs, J. B. Nasrallah, M. E. Nasrallah, Independent S-Locus Mutations Caused Self-Fertility in Arabidopsis thaliana. *PLoS Genet.* **5**, e1000426 (2009).
40. S. Fujii, *et al.*, Parallel evolution of dominant pistil-side self-incompatibility suppressors in Arabidopsis. *Nat. Commun. 2020 111* **11**, 1–9 (2020).
41. O. Voinnet, Origin, Biogenesis, and Activity of Plant MicroRNAs. *Cell* **136**, 669–687 (2009).
42. X.-J. He, *et al.*, NRPD4, a protein related to the RPB4 subunit of RNA polymerase II, is a component of RNA polymerases IV and V and is required for RNA-directed DNA methylation. *Genes Dev.* **23**, 318–330 (2009).
43. S. W.-L. Chan, *et al.*, RNA Silencing Genes Control de Novo DNA Methylation. *Science* 303, 1336–1336 (2004).
44. D. R. Masser, A. S. Berg, W. M. Freeman, Focused, high accuracy 5-methylcytosine quantitation with base resolution by benchtop next-generation sequencing. *Epigenetics Chromatin* **6**, 33 (2013).
45. S. Mi, *et al.*, Sorting of Small RNAs into Arabidopsis Argonaute Complexes Is Directed by the 5′ Terminal Nucleotide. *Cell* **133**, 116–127 (2008).
46. A. Le Vève, "Balancing selection, genetic load and dominance between self-incompatibility alleles in Arabidopsis : an empirical and theoretical study of this ménage à trois," Université de Lille (2022-....). (2022).
47. H. Liu, *et al.*, Nuclear functions of mammalian MicroRNAs in gene regulation, immunity and cancer. *Mol. Cancer* **17**, 64 (2018).
48. J. O'Brien, H. Hayder, Y. Zayed, C. Peng, Overview of MicroRNA Biogenesis, Mechanisms of Actions, and Circulation. *Front. Endocrinol.* **9** (2018).
49. T. C. Roberts, The MicroRNA Biology of the Mammalian Nucleus. *Mol. Ther. - Nucleic Acids* **3** (2014).
50. P. Hoffer, *et al.*, Posttranscriptional gene silencing in nuclei. *Proc. Natl. Acad. Sci.* **108**, 409–414 (2011).
51. N. G. Bologna, *et al.*, Nucleo-cytosolic Shuttling of ARGONAUTE1 Prompts a Revised Model of the Plant MicroRNA Pathway. *Mol. Cell* **69**, 709-719.e5 (2018).
52. Y. Fang, D. L. Spector, Identification of Nuclear Dicing Bodies Containing Proteins for MicroRNA Biogenesis in Living Arabidopsis Plants. *Curr. Biol.* **17**, 818–823 (2007).
53. W. Wang, *et al.*, An Importin β Protein Negatively Regulates MicroRNA Activity in Arabidopsis[W]. *Plant Cell* **23**, 3565–3576 (2011).
54. N. Baumberger, D. C. Baulcombe, *Arabidopsis* ARGONAUTE1 is an RNA Slicer that selectively recruits microRNAs and short interfering RNAs. *Proc. Natl. Acad. Sci.* **102**, 11928–11933 (2005).
55. J. Dolata, *et al.*, Salt Stress Reveals a New Role for ARGONAUTE1 in miRNA Biogenesis at the

Transcriptional and Posttranscriptional Levels. *Plant Physiol.* **172**, 297–312 (2016).

56. E. J. Finnegan, D. Liang, M.-B. Wang, Self-incompatibility: Smi silences through a novel sRNA pathway. *Trends Plant Sci.* **16**, 238–241 (2011).
57. S. Fujii, K. Kubo, S. Takayama, Non-self- and self-recognition models in plant self-incompatibility. *Nat. Plants* **2**, 1–9 (2016).
58. H. Zhao, *et al.*, Origin, loss, and regain of self-incompatibility in angiosperms. *Plant Cell* **34**, 579–596 (2022).
59. H. Bastide, S. V. Saenko, M. Chouteau, M. Joron, V. Llaurens, Dominance mechanisms in supergene alleles controlling butterfly wing pattern variation: insights from gene expression in Heliconius numata. *Heredity* **130**, 92–98 (2023).
60. M. Joron, C. D. Jiggins, A. Papanicolaou, W. O. McMillan, Heliconius wing patterns: an evo-devo model for understanding phenotypic diversity. *Heredity* **97**, 157–167 (2006).
61. R. J. Stein, *et al.*, Relationships between soil and leaf mineral composition are element-specific, environment-dependent and geographically structured in the emerging model Arabidopsis halleri. *New Phytol.* **213**, 1274–1286 (2017).
62. S. J. Clough, A. F. Bent, Floral dip: A simplified method for Agrobacterium-mediated transformation of Arabidopsis thaliana. *Plant J.* **16**, 735–743 (1998).
63. H.-L. Xing, *et al.*, A CRISPR/Cas9 toolkit for multiplex genome editing in plants. *BMC Plant Biol.* **14**, 327 (2014).
64. Z.-P. Wang, *et al.*, Egg cell-specific promoter-controlled CRISPR/Cas9 efficiently generates homozygous mutants for multiple target genes in Arabidopsis in a single generation. *Genome Biol.* **16**, 144 (2015).
65. S. Lahmy, *et al.*, Evidence for ARGONAUTE4–DNA interactions in RNA-directed DNA methylation in plants. *Genes Dev.* **30**, 2565–2570 (2016).
66. C.-G. Duan, *et al.*, Specific but interdependent functions for Arabidopsis AGO4 and AGO6 in RNA-directed DNA methylation. *EMBO J.* **34**, 581–592 (2015).
67. S. M. Smith, P. J. Maughan, SNP genotyping using KASPar assays. *Methods Mol. Biol. Clifton NJ* **1245**, 243–256 (2015).
68. M. W. Pfaffl, A new mathematical model for relative quantification in real-time RT-PCR. *Nucleic Acids Res.* **29**, 45e–445 (2001).
69. C. Barre-Villeneuve, *et al.*, The unique dual targeting of AGO1 by two types of PRMT enzymes promotes phasiRNA loading in Arabidopsis thaliana. *Nucleic Acids Res.* gkae045 **(2024)**. https://doi.org/10.1093/nar/gkae045.
70. F. Krueger, TrimGalore. (2016). Deposited 2016.
71. M. J. Axtell, ShortStack: Comprehensive annotation and quantification of small RNA genes. *RNA* **19**, 740 **(2013)**.
72. Z. Gu, Complex heatmap visualization. *iMeta* **1**, e43 (2022).
73. Z. Gu, L. Gu, R. Eils, M. Schlesner, B. Brors, circlize implements and enhances circular visualization in R. *Bioinformatics* **30**, 2811–2812 (2014).
74. C. Belser, *et al.*, Chromosome-scale assemblies of plant genomes using nanopore long reads

and optical maps. *Nat. Plants* **4**, 879–887 (2018).

75. Y. Chen, *et al.*, Efficient assembly of nanopore reads via highly accurate and intact error correction. *Nat. Commun.* **12**, 60 (2021).
76. R. Vaser, I. Sović, N. Nagarajan, M. Šikić, Fast and accurate de novo genome assembly from long uncorrected reads. *Genome Res.* **27**, 737–746 (2017).
77. J.-M. Aury, B. Istace, Hapo-G, haplotype-aware polishing of genome assemblies with accurate reads. *NAR Genomics Bioinforma.* **3**, lqab034 (2021).
78. S. Huang, M. Kang, A. Xu, HaploMerger2: rebuilding both haploid sub-assemblies from high-heterozygosity diploid genome assembly. *Bioinformatics* **33**, 2577–2579 (2017).
79. V. Solovyev, P. Kosarev, I. Seledsov, D. Vorobyev, Automatic annotation of eukaryotic genes, pseudogenes and promoters. *Genome Biol.* **7**, S10 (2006).
80. V. Llaurens, *et al.*, Does frequency-dependent selection with complex dominance interactions accurately predict allelic frequencies at the self-incompatibility locus in Arabidopsis halleri? *Evolution* **62**, 2545–2557 (2008).
81. D. Gaio, *et al.*, Hackflex: low cost Illumina Nextera Flex sequencing library construction. *bioRxiv* 779215 (2021). https://doi.org/10.1101/779215.
82. M. D. Schultz, *et al.*, Human body epigenome maps reveal noncanonical DNA methylation variation. *Nature* **523**, 212–216 (2015).
83. R Core Team, R: A Language and Environment for Statistical Computing | BibSonomy. (2017). Available at: https://www.R-project.org/.
84. H. Wickham, *ggplot2: Elegant Graphics for Data Analysis* (Springer, 2009).
85. F. Krueger, S. R. Andrews, Bismark: a flexible aligner and methylation caller for Bisulfite-Seq applications. *Bioinformatics* **27**, 1571–1572 (2011).

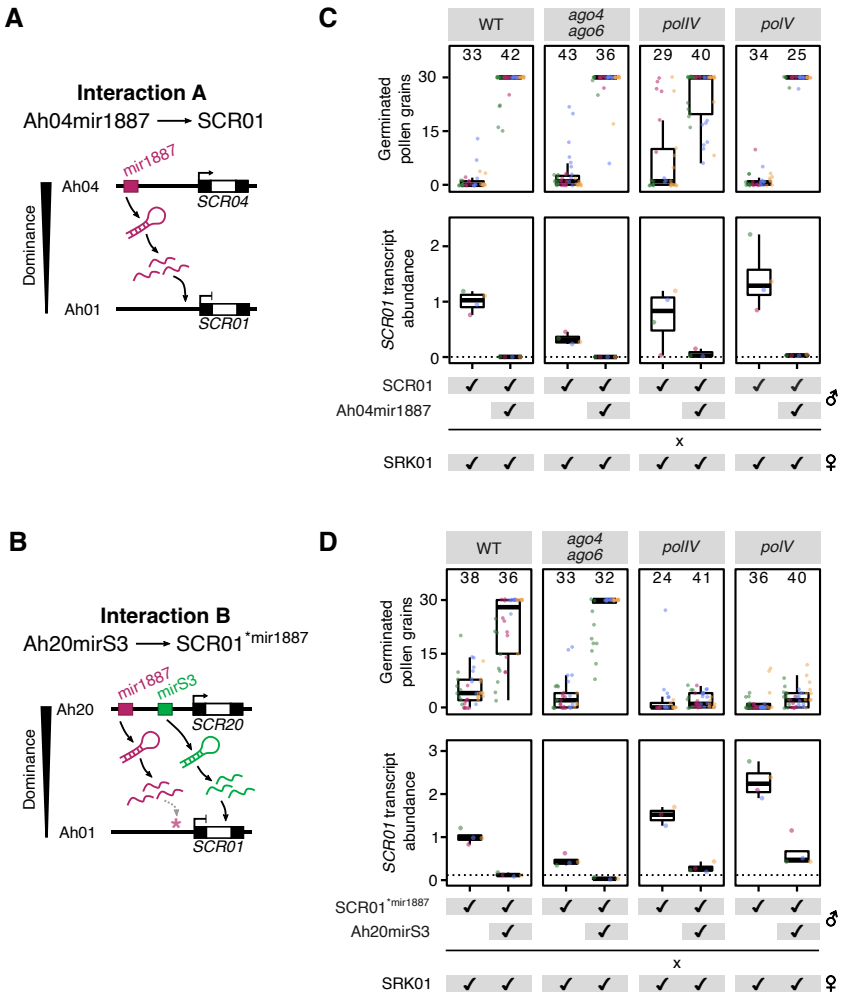

Figure 1. The RdDM pathway is not required for the activity of Ah04mir1887 and Ah20mirS3.

(A,B) Dominance interactions studied in this paper. The black and white regions within *SCR* genes correspond to exons and introns, respectively. **(A)** Interaction A focuses on the role of the sRNA precursor Ah04mir1887 in mediating the dominance of Ah04 over Ah01. **(B)** Interaction B focuses on the role of Ah20mirS3 in mediating the dominance of Ah20 over Ah01. *S*-locus sRNA precursors consist of inverted repeats that form hairpins which are processed into multiple sRNAs showing sequence homology to specific *SCR* regions: Ah04mir1887 sRNAs show homology to the 5' region region of *SCR01*, while Ah20mirS3 sRNAs show homology to the intronic region (white) of *SCR01*. Because sRNAs produced from the Ah20mir1887 precursor show homology to the wt *SCR01* 5' region region, and to study the specific effect of Ah20mirS3 in Interaction B, the *SCR01*^{*mir1887} line containing five point mutations in the *SCR01* 5' region was created, which disrupts the homology with Ah20mir1887 sRNAs. **(C,D)** Phenotypic and expression assay evaluating the role of key RdDM components on the action of Ah04mir1887 **(C)**, and Ah20mirS3 **(D)**. Crosses between *SRK01*-expressing mothers and *SCR01*-expressing fathers were performed in wt and RdDM mutant backgrounds in the absence or presence of the respective sRNA precursor. The number of germinated pollen grains of the indicated genotype was counted on pistils of SRK01 mothers. *SCR01* expression in immature buds of the indicated genotype was measured by RT-qPCR and normalized to the wt level. Five biological replicates

(represented by the differently colored dots) were analyzed for pollen germination and *SCR01* expression. Numbers on top of columns indicate the total number of siliques sampled for pollen germination assays.

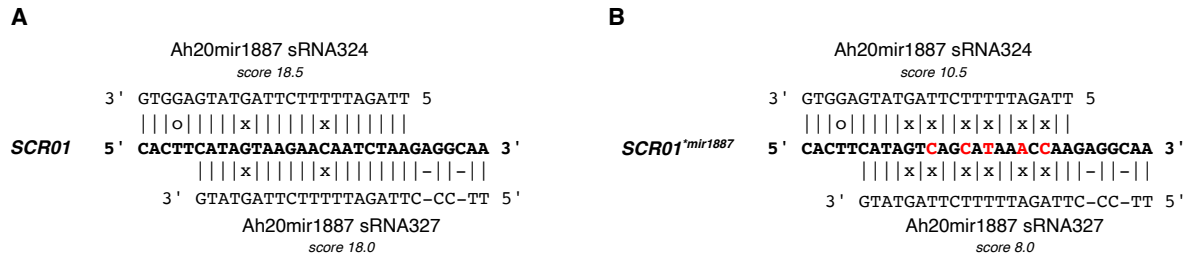

Figure 1 S1. *SCR01*^{*mir1887} transgenic line

(A) Alignment between the native mir1887 target site on *SCR01* and Ah20mir1887 sRNAs with a targeting score ≥ 18. **(B)** Alignment between the same sRNAs and the mutated mir1887 target site of the transgenic line *SCR01*^{*mir1887}. Note that the mutations decrease the homology score below 18, suggesting that these sRNAs are not able to target the mutated site. Mutated sites are in red.

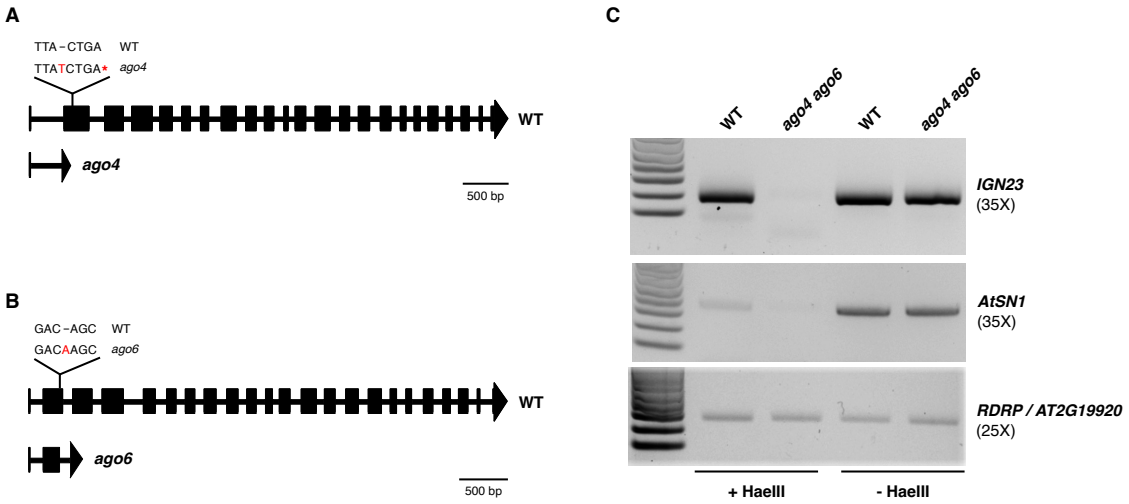

Figure 1 S2. Validation of the RdDM CRISPR/Cas9 mutants generated in this study.

(A-B) Schematic representation of CRISPR/Cas9 induced mutations in the *AGO4* and *AGO6* genes. Sequence changes are shown in red, premature stop codons are represented by the asterisk. **(C)** Chop-PCR assay on wt C24 plants and *ago4 ago6* double mutant plants. *IGN23* and *AtSN1* correspond to RdDM-dependent methylated regions, while *RDRP* corresponds to a non-methylated region.

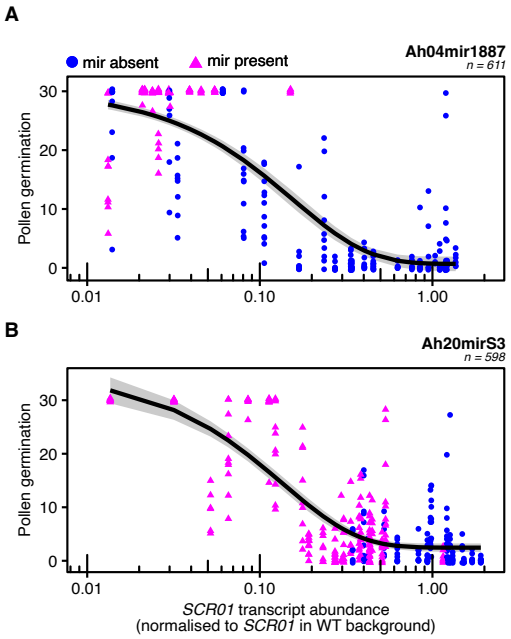

Figure 1 S3. A compatible pollen germination phenotype requires a low *SCR01* transcript abundance.

Non-linear regression analysis modeling the relationship between *SCR01* transcript abundance levels and pollen germination. For both Ah04mir1887 **(A)** and Ah20mirS3 **(B)** sRNA precursors a compatible pollen germination phenotype (~20-30 pollen grains) requires a 10-fold decrease in *SCR01* transcript abundance (compared to the level observed in the wt). Analysis was performed using the phenotypic and expression data presented in **Fig. 1 C-D**. The black line represents the predicted model and the gray area corresponds to the 95% confidence interval.

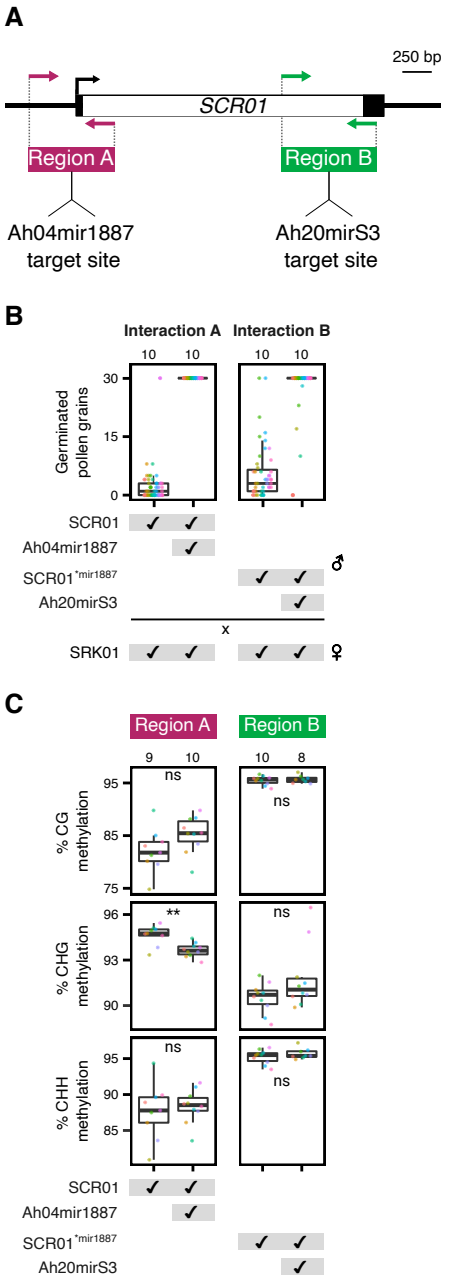

867 **Figure 1 S4. Ah04mir1887 and Ah20mirS3 are not associated with detectable DNA methylation**
868 **changes at *SCR01* target sites.**

869 **(A)** Schematic representation of the BSAS assay performed to measure DNA methylation at the
870 Ah04mir1887 target site (*SCR01* 5' region - Region A), and at the Ah20mirS3 target site (*SCR01* intron
871 - Region B). Region A and Region B correspond to fragments of 794 and 871 bp, respectively, centered
872 in each sRNA precursor's target site. **(B)** Phenotypic validation of lines used for the BSAS assay.
873 Colored dots correspond to values obtained for each biological replicate. Number of biological replicates
874 is indicated at the top of the panel. For each biological replicate pollen germination on a total of 5 *SRK01*
875 pistils was counted. **(C)** Average DNA methylation levels on Region A (Interaction A) and Region B
876 (Interaction B) of *SCR01*. DNA methylation levels correspond to the average of methylation in all

877 cytosines in the top and bottom DNA strands of sampled regions. Number of biological replicates is
878 indicated at the top of the panel. Statistical differences were assessed using a two-tailed Mann-Whitney
879 test with continuity correction (ns - non significant, p-value > 0.05; ** - p-value ≤ 0.01).

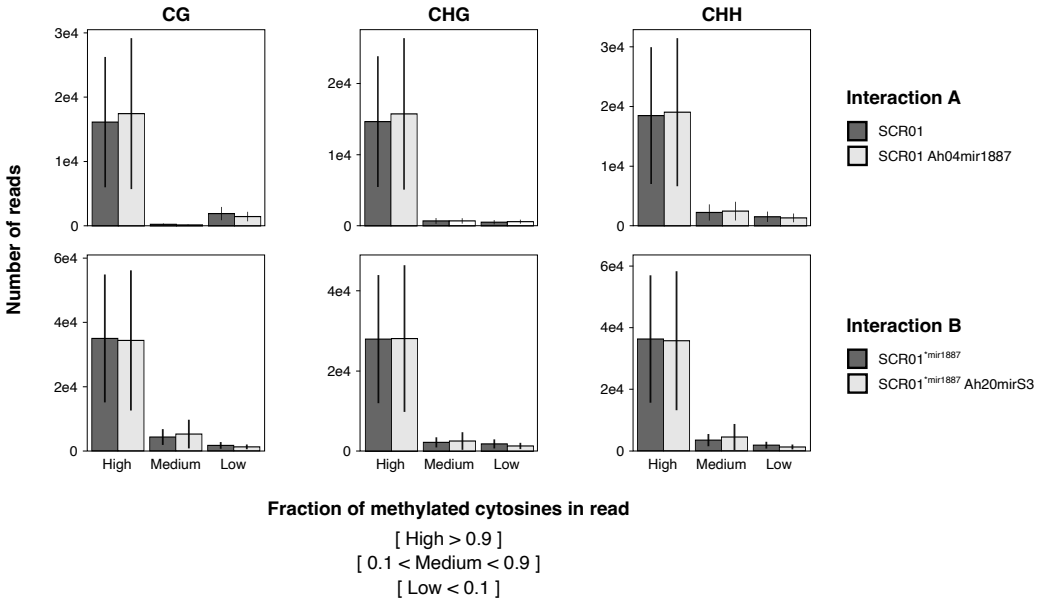

Figure 1 S5. Ah04mir1887 and Ah20mirS3 target sites are heavily methylated.

BSAS reads were grouped according to the fraction of methylated cytosines within each read. High: reads where nearly all cytosine positions are methylated (> 90% cytosines); Low: reads where very few cytosine positions are methylated (< 10% cytosines); Medium: all reads with more than 10% and less that 90% cytosines methylated. Error bars represent the standard deviation between replicates. No statistically significant differences were detected in the number of highly and lowly methylated reads between the *SCR01* and *SCR01* Ah04mir1887 or *SCR01*mir1887* and *SCR01*mir1887* Ah20mirS3 genotypes (p-value > 0. 05, two-tailed Mann-Whitney test with continuity correction).

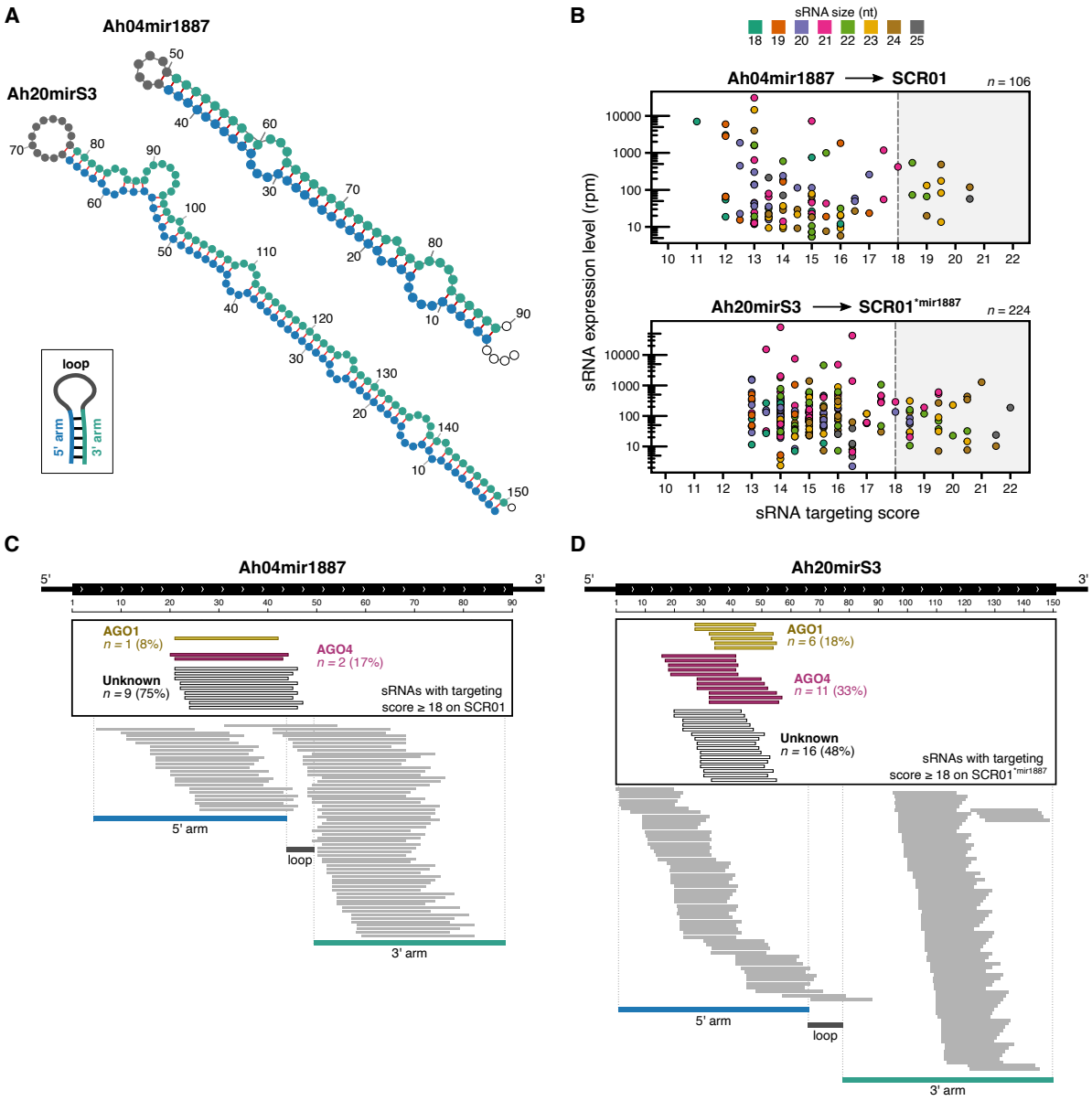

Figure 2. Ah04mir1887 and Ah20mirS3 hairpins are processed into numerous sRNAs.

(A) Predicted RNA hairpin structures of the *S*-locus sRNA precursors Ah04mir1887 and Ah20mirS3. **(B)** Expression of Ah04mir1887 and Ah20mirS3 sRNAs as a function of their targeting score against *SCR01*. The color of the dots corresponds to the size of the sRNA. The grey box highlights sRNAs predicted to induce a reduction in *SCR01* transcript abundance (score ≥ 18). *n* corresponds to the total number of unique sRNAs identified upon sequencing for each sRNA precursor. **(C-D)** Genomic representation of the Ah04mir1887 and Ah20mirS3 loci, and their respective sRNAs. The black rectangle highlights sRNAs predicted to induce a reduction in *SCR01* transcript abundance (score ≥ 18). AGO loading information for each functional sRNA is indicated by the sRNA color (yellow – sRNA loaded predominantly in AGO1; magenta – sRNA loaded predominantly in AGO4; white – sRNAs with unknown loading profile), **see section *ARGONAUTE immunoprecipitation and sRNA sequencing*** for more details.

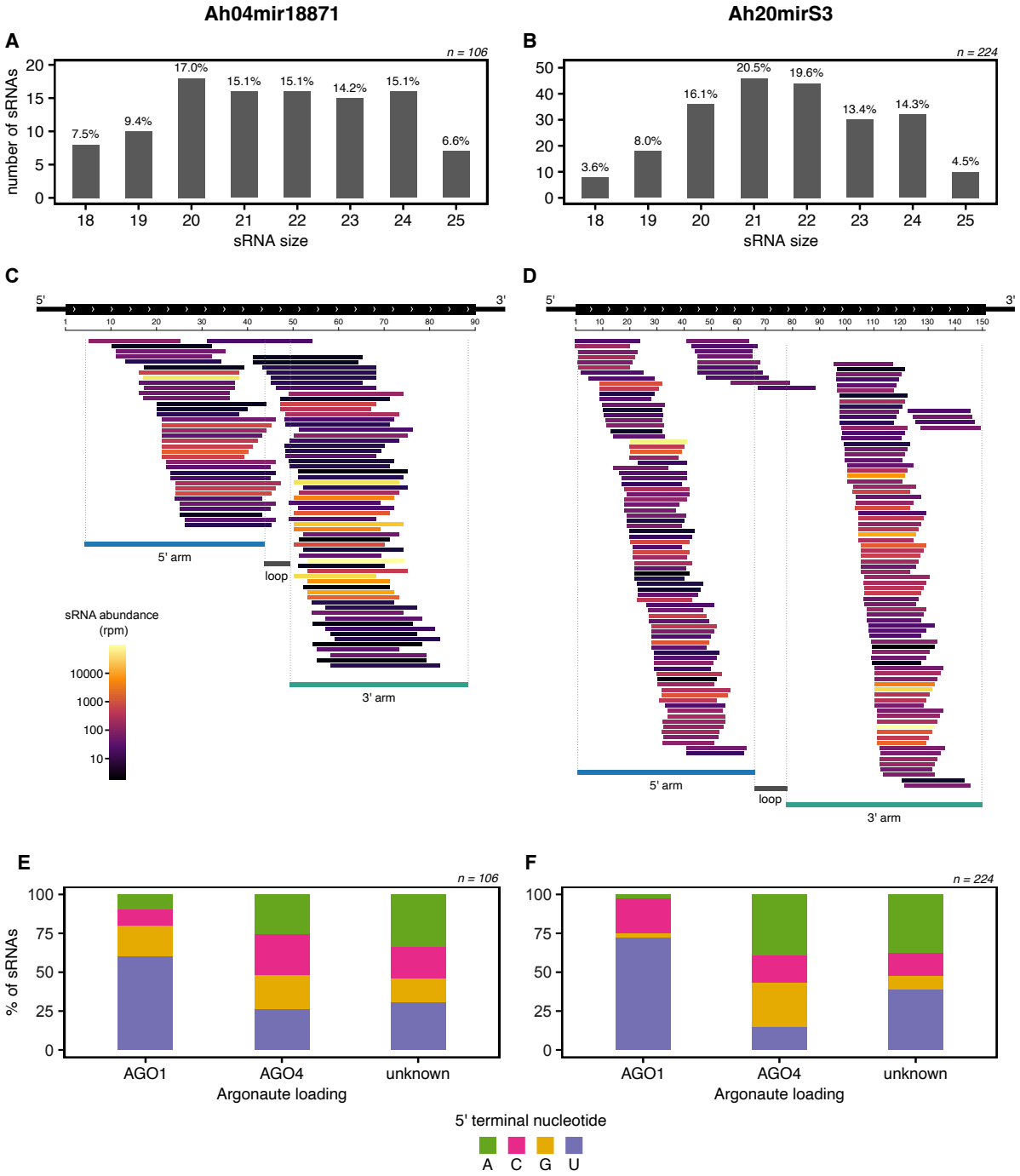

Figure 2 S1. sRNAs produced from Ah04mir1887 and Ah20mirS3 do not show a specific size bias but vary in their abundance levels.

Size distribution of sRNAs derived from Ah04mir1887 **(A)** and Ah20mirS3 **(B)**. **(C-D)** Genomic representation of the Ah04mir1887 and Ah20mirS3 loci, and their respective sRNAs. sRNAs are colored according to their abundance level. **(E-F)** 5' terminal nucleotide frequencies in Ah04mir1887 and Ah20mirS3 sRNAs, related to their inferred AGO loading pattern.

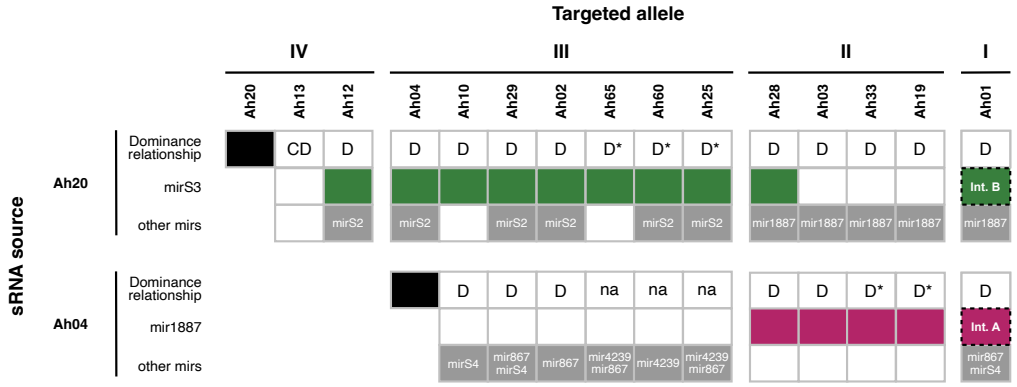

906 Figure 3. Ah04mir1887 and Ah20mirS3 underlie numerous *S*-allele dominance interactions.

907 Schematic representation of the dominance relationship between alleles Ah20, Ah04 and other *S*-
908 alleles in the current *A. halleri* dominance network. The dominance phenotypes observed are
909 represented by D (dominant, as determined by phenotypic assays), CD (codominant, as determined by
910 phenotypic assays), and na (no phenotypic data available). D* refers to a predicted dominance
911 relationship, based on the difference between the dominance class of the sRNA source and the targeted
912 allele (15, 24). The sRNA precursors underlying each dominance relationship are highlighted in green
913 (mirS3), magenta (mir1887), or grey (other mirs). The specific interactions studied earlier in this
914 manuscript – Interaction A and Interaction B - are highlighted by a dashed box.

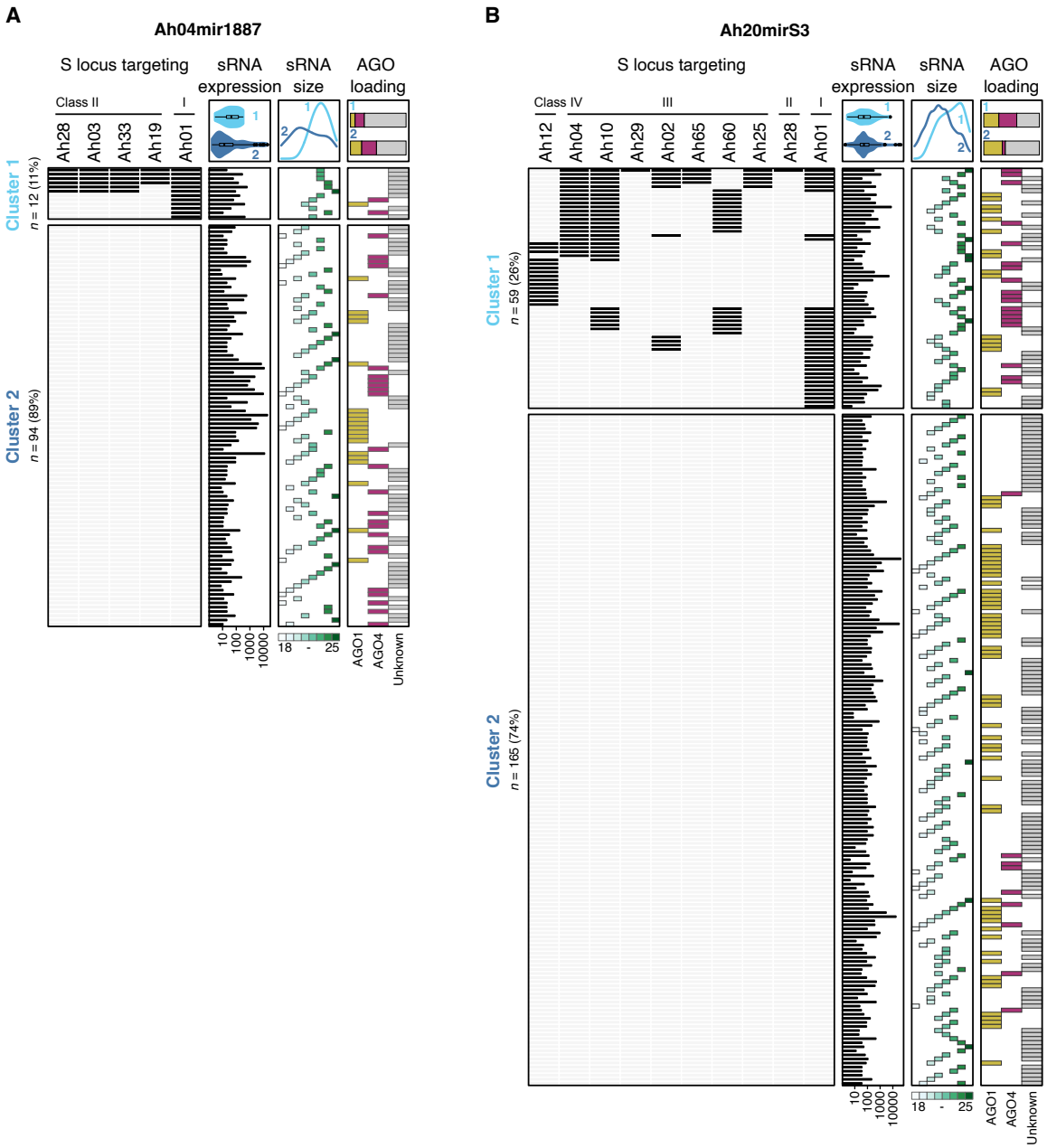

Figure 4. Ah04mir1887 and Ah20mirS3 produce multiple sRNAs targeting one or more *S*-alleles.

Heatmap representing the *S*-loci targeted by Ah04mir1887-derived sRNAs **(A)** and Ah20mirS3-derived sRNAs **(B)**. A black rectangle indicates that a specific sRNA has a targeting score of ≥ 18 against the corresponding *S*-allele. Cluster 1 groups sRNAs that target at least one *S*-allele, while Cluster 2 groups sRNAs that have no targets in the represented *S*-alleles. sRNA expression levels, sRNA size and AGO loading patterns are indicated for each sRNA. Summary plots comparing these features in Cluster 1 and Cluster 2 are shown in the top panel. *n* corresponds to the number of sRNAs produced by each sRNA precursor.

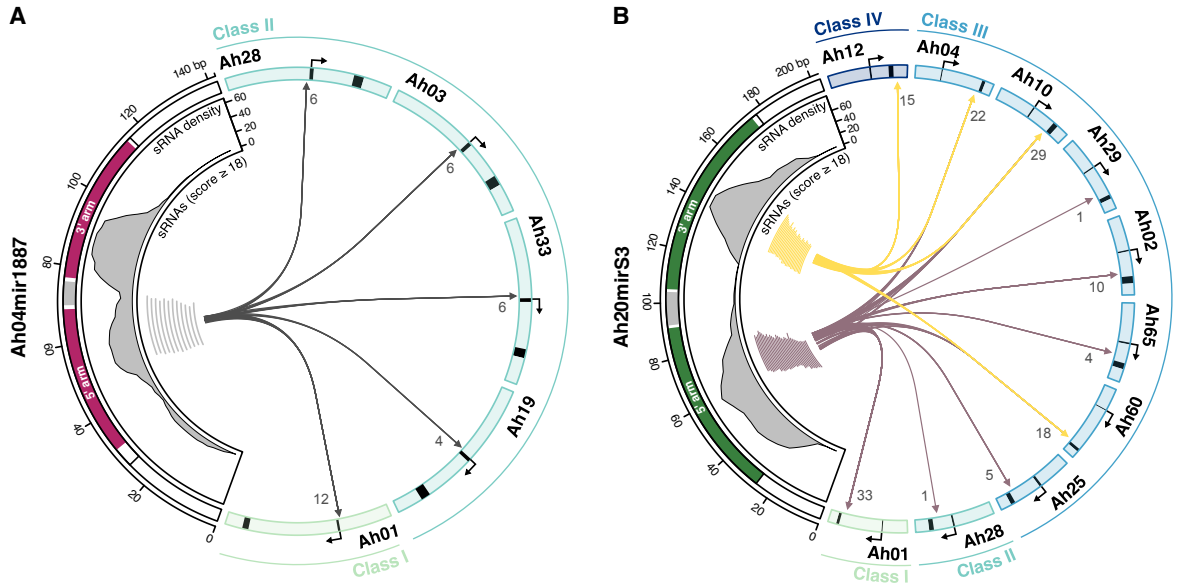

Figure 5. The targeting repertoire of *S*-locus sRNA precursors is enhanced by their heterogeneous processing pattern.

Circos plot representing the positional relationship between sRNAs produced by Ah04mir1887 **(A)**, Ah20mirS3 **(B)** and the corresponding targeted *S*-alleles. The genomic regions harboring Ah04mir1887 and Ah20mirS3 are represented on the left side of the plots. The predicted 5' and 3' hairpin arms are represented in magenta (Ah04mir1887) and green (Ah20mirS3), and the sRNA density (number of sRNAs) is plotted along the sRNA precursor region. Individual sRNAs with a score of ≥ 18 are represented by the grey, yellow or dark purple segments. Arrowed segments represent the sRNA source - target relationship. The numbers at the end of these arrowed segments indicate the total number of sRNAs targeting that respective allele. The *SCR* genomic region of targeted *S*-alleles is represented on the right side and includes 1500 bp upstream of the TSS and 500 bp downstream of the TES. *SCR* exons 1 and 2 are colored in black.